Sox2 and FGF20 interact to regulate organ of Corti hair cell and supporting cell development in a spatially-graded manner

Short title: Sox2 and FGF20 in cochlea development

Lu M. Yang[1], Kathryn S.E. Cheah[2], Sung-Ho Huh[1,3,*], David M. Ornitz[1,*]

[1]Department of Developmental Biology; Washington University School of Medicine; St. Louis, Missouri, 63110; USA

[2]School of Biomedical Sciences; The University of Hong Kong; Pokfulam, Hong Kong, China

[3]Holland Regenerative Medicine Program, and the Department of Neurological Sciences; University of Nebraska Medical Center; Omaha, Nebraska, 68198; USA

*Corresponding authors

Email: dornitz@wustl.edu (D.M.O.), sungho.huh@unmc.edu (S.H.)

Author contributions

Conceptualization, L.M.Y., S.H., and D.M.O.; Methodology, L.M.Y., S.H., and D.M.O.; Formal Analysis, L.M.Y. and S.H.; Investigation: L.M.Y. and S.H.; Resources: K.S.E.C., S.H., and D.M.O.; Writing – Original Draft: L.M.Y. and D.M.O.; Writing – Review & Editing: L.M.Y., K.S.E.C., S.H., and D.M.O.; Supervision: D.M.O.; Funding Acquisition: S.H. and D.M.O.

Abstract

The mouse organ of Corti develops in two steps: progenitor specification and differentiation. Fibroblast Growth Factor (FGF) signaling is important in this developmental pathway, as deletion of FGF receptor 1 (*Fgfr1*) or its ligand, *Fgf20*, leads to the loss of hair cells and supporting cells from the organ of Corti. However, whether FGF20-FGFR1 signaling is required during specification or differentiation, and how it interacts with the transcription factor Sox2, also important for hair cell and supporting cell development, has been a topic of debate. Here, we show that while FGF20-FGFR1 signaling functions during progenitor differentiation, FGFR1 has an FGF20-independent, Sox2-dependent role in specification. We also show that a combination of reduction in *Sox2* expression and *Fgf20* deletion recapitulates the *Fgfr1*-deletion phenotype. Furthermore, we uncovered a strong genetic interaction between *Sox2* and *Fgf20*, especially in regulating the development of hair cells and supporting cells towards the basal end and the outer compartment of the organ of Corti. To explain this genetic interaction and its effects on the basal end of the organ of Corti, we provide evidence that decreased *Sox2* expression delays specification, which begins at the organ of Corti apex, while *Fgf20*-deletion results in premature onset of differentiation, which begins near the organ of Corti base. Thereby, *Sox2* and *Fgf20* interact to ensure that specification occurs before differentiation towards the cochlear base. These findings reveal an intricate developmental program regulating organ of Corti development along the basal-apical axis of the cochlea.

Author summary

The mammalian cochlea contains the organ of Corti, a specialized sensory epithelium populated by hair cells and supporting cells that detect sound. Hair cells are susceptible to injury by noise,

toxins, and other insults. In mammals, hair cells cannot be regenerated after injury, resulting in permanent hearing loss. Understanding genetic pathways that regulate hair cell development in the mammalian organ of Corti will help in developing methods to regenerate hair cells to treat hearing loss. Many genes are essential for hair cell and supporting cell development in the mouse organ of Corti. Among these are *Sox2*, *Fgfr1*, and *Fgf20*. Here, we investigate the relationship between these three genes to further define their roles in development. Interestingly, we found that *Sox2* and *Fgf20* interact to affect hair cell and supporting cell development in a spatially-graded manner. We found that cells toward the outer compartment and the base of the organ of Corti are more strongly affected by the loss of *Sox2* and *Fgf20*. We provide evidence that this spatially-graded effect can be partially explained by the roles of the two genes in the precise timing of two sequential stages of organ of Corti development, specification and differentation.

Introduction

The inner ear contains six sensory organs required for the senses of hearing and balance. The cochlea, a snail-like coiled duct, is the auditory organ. It contains specialized sensory epithelia, called the organ of Corti, composed of hair cells (HCs) and supporting cells (SCs). In mammals, this sensory epithelium is elegantly patterned, with one row of inner hair cells (IHCs) and three rows of outer hair cells (OHCs), separated by two rows of pillar cells forming the tunnel of Corti. Each row of OHCs is associated with a row of supporting cells called Deiters' cells. Here, we refer to pillar cells and Deiters' cells collectively as SCs.

Organ of Corti development has been described as occurring in two main steps: prosensory specification and differentiation [1]. During prosensory specification, proliferative progenitors at

73 the floor of the developing cochlear duct are specified and exit the cell cycle to form the
74 postmitotic prosensory domain. Here, we define specification to be a process that makes
75 progenitors competent to differentiate. We also use cell cycle exit as a marker for specified cells
76 in the prosensory domain (prosensory cells). During differentiation, prosensory cells differentiate
77 into both HCs and SCs [2]. Interestingly, cell cycle exit, marking the completion of specification,
78 and initiation of differentiation occur in waves that travel in opposite directions along the length
79 of the cochlear duct. At around embryonic day 12.5 (E12.5) in the mouse, progenitors begin to
80 exit the cell cycle and express the cyclin-dependent kinase inhibitor CDKN1B ($p27^{Kip1}$) in a wave
81 that begins at the apex of the cochlea (the cochlear tip) and reaches the base of the cochlea by
82 around E14.5 [3,4]. Afterwards, the specified prosensory cells begin differentiating into HCs and
83 SCs in a wave that begins at the mid-base at around E13.5, and spreads quickly to the rest of
84 the base and to the apex over the next few days [1]. Notably, while the basal end of the
85 cochlear duct differentiates immediately after prosensory specification, the apical end has a
86 longer time between specification and differentiation, providing a larger “temporal buffer” for
87 apical development. The spiral ganglion, containing neurons synapsing to HCs, has been
88 shown to be important for this delay in apical differentiation, via Sonic Hedgehog (SHH)
89 signaling [5–8].
90
91 The transcription factor *Sox2* is one of the earliest markers of prosensory cells [9,10]. Mice with
92 specific *Sox2* hypomorphic mutations that affect inner ear expression have hearing impairment
93 due to decreased HC and SC number, while mice with inner ear-specific *Sox2* null mutations
94 are completely deaf and have no HCs or SCs [11,12]. Genetic experiments show that *Sox2* is
95 both necessary and sufficient for prosensory specification. Absence of *Sox2* expression leads to
96 the loss of *Cdkn1b* expression at E14, a marker for the prosensory domain [12], while ectopic
97 *Sox2* expression in cochlear nonsensory epithelium can induce ectopic sensory patches [13–
98 15].

99

100 The Fibroblast Growth Factor (FGF) signaling pathway also plays vital roles in organ of Corti
101 development [16]. Studies utilizing cochlear explants showed that inhibition of FGF signaling
102 prior to and during stages of HC and SC differentiation results in decreased HC and SC number
103 [17]. Signaling through FGF receptor 1 (FGFR1), in particular, is essential during this process.
104 Conditional deletion of *Fgfr1* (Fgfr1-CKO) in the developing cochlear epithelium resulted in
105 dramatically reduced HC and SC number [18–20]. This has been attributed to decreased *Sox2*
106 expression in the prosensory domain of Fgfr1-CKO mice, leading to a defect in prosensory
107 specification [19].
108
109 FGF20 has been hypothesized to be the FGFR1 ligand during organ of Corti development. Both
110 *in vitro* inhibition of FGF20 with an anti-FGF20 antibody [17] and *in vivo* knockout of *Fgf20*
111 (Fgf20-KO) [21] led to decreased HC and SC number, similar to the Fgfr1-CKO phenotype.
112 However, the Fgf20-KO phenotype is clearly not as severe as that of Fgfr1-CKO. Almost all
113 OHCs and some IHCs are missing in Fgfr1-CKO mice [19], while only 2/3 of OHCs are missing
114 in Fgf20-KO mice, without any loss of IHCs [21]. This suggests that another FGF ligand may be
115 redundant with and compensating for the loss of FGF20, the identity of which is currently
116 unknown.

117 Another difference between Fgfr1-CKO and Fgf20-KO mice is the proposed mechanism
118 accounting for the decrease in HCs and SCs. Interestingly, unlike in Fgfr1-CKO mice, Sox2
119 expression in the prosensory domain is not disrupted in Fgf20-KO mice [19,21]. Rather, FGF20
120 seems to function during HC and SC differentiation. These differences between the Fgfr1-CKO
121 and Fgf20-KO phenotypes and their relationship with *Sox2* suggest that FGF20/FGFR1
122 signaling has a more complex and as yet unexplained role during organ of Corti development.
123

124 Here, we hypothesize that FGFR1 signaling has functions in both steps of organ of Corti
125 development: an earlier role in prosensory specification that involves *Sox2*, and a later role in
126 the initiation of differentiation. We provide evidence that FGF20 regulates differentiation but not
127 specification. Moreover, while *Fgfr1* functions upstream of *Sox2*, *Fgf20* is downstream of *Sox2*.
128 We further show that *Sox2* and *Fgf20* genetically interact during organ of Corti development.
129 Interestingly, downregulation of both genes leads to the loss of hair cells and supporting cells
130 preferentially towards the outer compartment and the basal end of the cochlear duct. To explain
131 the more severe basal phenotype, we provide evidence that *Sox2* regulates the timing of
132 prosensory specification, while *Fgf20* regulates the timing of differentiation. As these two steps
133 occur along a developmental pathway, we hypothesize that prosensory specification must occur
134 prior to differentiation. In *Sox2* hypomorphic mice, prosensory specification is delayed, while in
135 Fgf20-KO mice, onset of differentiation occurs prematurely. When combined, these two defects
136 led to differentiation attempting to initiate prior to the completion of specification towards the
137 basal end of the cochlear duct. These results define unique functions of and complex
138 interactions among FGF20, FGFR1, and Sox2 during organ of Corti development and highlight
139 the potential importance of the timing of specification and differentiation along different regions
140 of the cochlear duct.
141

142 ## Results

143

144 ### The Fgf20-KO cochlear phenotype is less severe than the Fgfr1-CKO phenotype

145

146 Previous studies showed that deletion of *Fgf20* leads to a loss of two thirds of OHCs in the
147 mouse organ of Corti [21], while conditional deletion of *Fgfr1* from the cochlear epithelium leads
148 to a loss of almost all OHCs and some IHCs [19,20]. To rule out the effect of genetic

149 background accounting for these differences, we generated *Fgf20* knockout (Fgf20-KO: *Fgf20*$^{-/-}$)
150 and *Fgfr1* conditional knockout (Fgfr1-CKO: *Foxg1*$^{Cre/+}$; *Fgfr1*$^{flox/-}$) mice along with littermate
151 controls (*Fgf20*$^{+/-}$ for Fgf20-KO and *Fgfr1*$^{flox/+}$, *Fgfr1*$^{flox/-}$, and *Foxg1*$^{Cre/+}$;*Fgfr1*$^{flox/+}$ for Fgfr1-CKO)
152 on a mixed C57BL/6J and 129X1/SvJ genetic background. Fgf20-KO and Fgfr1-CKO mice were
153 generated in separate matings; therefore, some genetic background differences could persist.
154 *Foxg1*^{Cre} targets most of the otic vesicle as early as E9.5 [22] and has been used in other
155 studies to conditionally delete *Fgfr1* [18–20]. In the *Fgf20*$^{-}$ allele, exon 1 of *Fgf20* is replaced by
156 a sequence encoding a GFP-Cre fusion protein [18]. We also refer to this null allele as *Fgf20*^{Cre}.
157
158 We examined the cochleae at P0 (Figs 1A and 1B) and quantified the length of the cochlear
159 duct and the total number of IHCs, OHCs, and SCs (Figs 1C-1F), as well as the number of cells
160 along the basal, middle, and apical turns of the cochlear duct (S1A-S1C Figs). Refer to Fig 1G
161 for the positions of basal, middle, and apical turns along the cochlear duct. We identified HCs
162 based on Phalloidin labeling and SCs based on Prox1/Sox2 labeling. IHCs and OHCs were
163 distinguished based on location relative to p75NTR-labeled inner pillar cells (IHCs are neural, or
164 towards the center of the coiled duct; OHCs are abneural).
165
166 In both Fgf20-KO and Fgfr1-CKO cochleae, there were gaps in the sensory epithelium that
167 lacked HCs and SCs along the entire cochlear duct. Quantitatively, Fgf20-KO cochleae had a
168 6% reduction in cochlear length compared to control (*Fgf20*$^{+/-}$) cochleae, while Fgfr1-CKO
169 cochleae had a 28% reduction compared to control (*Fgfr1*$^{Cre/+}$;*Fgfr1*$^{flox/+}$). Fgf20-KO did not have
170 a significant reduction in the number of IHCs, while Fgfr1-CKO cochleae had a 40% reduction.
171 Fgf20-KO cochleae only had a 76% reduction in the number of OHCs, while Fgfr1-CKO
172 cochleae had almost a complete lack of OHCs, a 97% reduction. For SCs, Fgf20-KO cochleae
173 had a 59% reduction, while Fgfr1-CKO cochleae had an 84% reduction. These patterns
174 persisted when HC and SC numbers were normalized to cochlear length. These results were all

175 consistent with previous studies [19,21] and showed that the Fgfr1-CKO phenotype is more
176 severe than the Fgf20-KO phenotype in cochlear length and in the number of HCs and SCs. We
177 hypothesize that during organ of Corti development, an additional FGFR1 ligand compensates
178 for the loss of FGF20.
179
180 Notably, while the total number of IHCs was decreased in Fgfr1-CKO cochleae, the decrease
181 was only observed in the basal and middle turns of the cochlea, not in the apical turn (S1A Fig).
182 In addition, the number of IHCs normalized to cochlear length was slightly increased in Fgf20-
183 KO cochleae (Fig 1D), and this increase was only prominent in the middle and apical turns of
184 the cochlea, but not in the basal turn (S1A Fig). The increase in IHCs could be explained by the
185 shortened cochlear duct length in Fgf20-KO mice. No such basal/middle/apical turn
186 discrepancies existed in the number of OHCs or SCs in either genotype (S1B and S1C Figs).
187
188 Our previous studies also noted that the apical tip of Fgf20-KO cochleae has delayed
189 differentiation relative to control at E16.5 and P0, but catches up by P7 [21]. We confirmed this
190 result, finding that at P0 in control cochleae, sensory epithelium at the apical tip has begun to
191 differentiate, based on phalloidin and p75NTR expression, while in Fgf20-KO cochleae, there
192 was no sign of differentiation at the apical tip. There was a similar delay in differentiation at the
193 apical tip of Fgfr1-CKO cochleae relative to control (S1E Fig). Refer to S1D Fig for the location
194 of the apical tip.
195
196 **FGFR1 but not FGF20 regulates *Sox2* expression**
197
198 Next, we examined *Sox2* expression in Fgf20-KO and Fgfr1-CKO cochleae at E14.5 by RNA in
199 situ hybridization and immunofluorescence. In control cochleae, *Sox2* mRNA and protein were
200 highly expressed in the prosensory domain (Fig 2A, refer to Fig 2C). The expression of *Sox2*

201 was not changed in Fgf20-KO cochleae compared to control; however, it was noticeably
202 decreased in Fgfr1-CKO cochleae (Fig 2A), in agreement with previous findings [19–21]. This
203 indicates that FGFR1 has an additional role, independent of FGF20, in regulating *Sox2*, which is
204 required for prosensory specification [12]. Similar to Sox2, CDKN1B expression in the
205 prosensory domain is also regulated by FGFR1, but not by FGF20 [18,19,21]. We confirmed
206 these results, finding that while CDKN1B expression was not changed in Fgf20-KO cochleae at
207 E14.5 relative to control, it was dramatically downregulated in Fgfr1-CKO cochleae (Fig 2B).
208 This is consistent with the role of Sox2 in regulating CDKN1B expression [12]. We hypothesize
209 that a yet unidentified FGF ligand (in addition to or independent of FGF20) signaling via FGFR1
210 regulates Sox2 expression (and therefore CDKN1B expression) during prosensory specification,
211 while FGF20 signaling via FGFR1 regulates differentiation (Fig 2D).
212
213 We also wanted to confirm that FGF20 signals to epithelial FGFR1 at around the initiation of
214 differentiation. To do so, we examined the expression of *Etv4* (also known as *Pea3*) and *Etv5*
215 (also known as *Erm*), two well-established downstream effectors of FGF signaling [23], by in situ
216 hybridization. The expression of these two genes are downregulated with FGF signaling
217 inhibition in E14 cochlear explants [17]. At E14.5, there were two domains of *Etv4* and *Etv5*
218 expression in control cochleae: the prosensory domain and the outer sulcus (S2A Fig,
219 brackets). The outer sulcus is the region of the cochlear epithelium abneural to the prosensory
220 domain at E14.5. In Fgf20-KO cochleae, expression of both genes was not detected in the
221 prosensory domain. In Fgfr1-CKO cochleae, expression of both genes was similarly not
222 detected in the prosensory domain. Expression of *Etv4* and *Etv5* in the outer sulcus was not
223 affected in Fgf20-KO and Fgfr1-CKO cochleae (S2A Fig). These results confirm that FGF20
224 signals through epithelial FGFR1 to the prosensory domain.
225

226 Previous studies have also reported a decrease in proliferation in Kölliker's organ (neural to the
227 prosensory domain, S2B Fig) in Fgfr1-CKO cochleae [20]. We replicated this result by
228 examining EdU (5-ethynyl-2'-deoxyuridine) incorporation at E14.5. *Fgfr1*-CKO mice had a
229 complete lack of EdU-incorporating Kölliker's organ cells, while Fgf20-KO mice did not show a
230 decrease in EdU incorporation (S2B Fig). This finding is also consistent with an additional FGF
231 ligand signaling via FGFR1, likely at an earlier stage. We do not know whether the proliferation
232 defect in Kölliker's organ contributes to the reduction in HC and SC number in Fgfr1-CKO mice.
233

234 **Genetic rescue of the Fgf20-KO phenotype suggests that FGF20 is required for**
235 **differentiation**

236

237 We have previously shown that recombinant FGF9, which is biochemically similar to FGF20
238 [23,24], is able to rescue the loss of HCs and SCs in Fgf20-KO explant cochleae [21].
239 Interestingly, while treatment with FGF9 at E13.5 and E14.5 was able to rescue the Fgf20-KO
240 phenotype, treatment at E15.5 was not. This temporal rescue specificity suggests that FGF20
241 signaling is required for the initiation of HC and SC differentiation.
242

243 To confirm the hypothesis that FGF20 is involved in differentiation and not specification (Fig
244 2D), we sought to more accurately determine the temporal requirement of FGF20 signaling. To
245 achieve this, we developed an *in vivo* genetic rescue model of the Fgf20-KO phenotype by
246 ectopically expressing FGF9. We combined $Fgf20^{Cre}$ with the $Fgf20^{\beta gal}$ [21], $ROSA^{rtTA}$ [25] and
247 TRE-Fgf9-IRES-eGfp [26] alleles to generate Fgf20-rescue ($Fgf20^{Cre/\beta gal}$;$ROSA^{rtTA/+}$;TRE-Fgf9-
248 IRES-eGfp) mice along with littermate controls: Fgf20-het ($Fgf20^{Cre/+}$;$ROSA^{rtTA/+}$), Fgf9-OA
249 ($Fgf20^{Cre/+}$;$ROSA^{rtTA/+}$;TRE-Fgf9-IRES-eGfp), and Fgf20-null ($Fgf20^{Cre/\beta gal}$;$ROSA^{rtTA/+}$). These
250 mice express the reverse tetracycline transactivator (rtTA) in the $Fgf20^{Cre}$ lineage, which

251 contains the prosensory domain and Kölliker's organ at E13.5 to E15.5 [18]. In mice expressing
252 TRE-Fgf9-IRES-eGfp, rtTA drives the expression of FGF9 upon doxycycline (Dox) induction.
253 The *Fgf20*$^{\beta gal}$ allele is another *Fgf20*-null allele, in which exon 1 of *Fgf20* is replaced by a
254 sequence encoding β-galactosidase. We combined *Fgf20*^{Cre} with *Fgf20*$^{\beta gal}$ to generate
255 homozygous mutant mice while maintaining a constant dosage of *Fgf20*^{Cre} in control and
256 knockouts.
257
258 Initially, pregnant dams were fed a Dox diet from E13.5 to E15.5 and pups were harvested at P0
259 to examine HC and SC development. As expected, Dox treatment itself did not appear to affect
260 HC or SC development in Fgf20-het and Fgf20-null cochleae, both of which showed the
261 expected phenotypes (Figs 3A and 3B). Ectopic expression of FGF9 during these stages also
262 did not affect HC or SC development in Fgf9-OA cochleae, showing that excess FGF20/FGF9
263 was not sufficient to produce ectopic HCs and SCs. Importantly, ectopic expression of FGF9
264 resulted in a full rescue of the number and patterning of HCs and SCs in Fgf20-rescue pups.
265 The organ of Corti in these rescue pups had one row of IHCs, three rows of OHCs, and five
266 rows of SCs throughout the entire length of the cochlear duct, without any gaps (Figs 3A and
267 3B). This shows that FGF20/FGF9 signaling at E13.5-E15.5 is sufficient for HC and SC
268 differentiation. The quantified results from all of the rescue experiments are summarized in Fig
269 3C, where the number of OHCs and SCs are represented as a percentage of that of Fgf20-het
270 mice treated with the same Dox regimen. All of the quantified data are presented in S3 Fig.
271
272 To more precisely determine the timing of rescue sufficiency, we fed pregnant dams Dox for a
273 period of 24 hours starting at E13.5, E14.5, or E15.5. With E13.5 Dox, patterning and OHC
274 number in the basal turn of the cochlea were completely rescued (Fig 3A). However, OHC
275 number in the middle and particularly the apical turns were only partially rescued, resulting in
276 regions with two rows of OHCs instead of three. For instance, in the apical turn, OHC number

277 was restored to 81% of Fgf20-het mice, which is statistically significantly increased compared to
278 Fgf20-null, but also statistically significantly decreased compared to Fgf20-het, indicating partial
279 rescue (Fig 3C). With E14.5 Dox, patterning and OHC number in the middle and apical turns
280 were completely rescued. However, OHC number in the basal turn was not completely rescued,
281 with regions of one or two rows of OHCs, instead of three. With E15.5 Dox, patterning and OHC
282 number was not rescued in the basal and middle turns, as gaps still formed between islands of
283 HCs (Fig 3A). However, OHC number in the apical turn was partially rescued, with two or three
284 rows of OHCs not separated by gaps towards the tip of the apex. In all of these experiments,
285 the rescue of SCs followed the same pattern as that of OHCs (Fig 3B).
286
287 These rescue results show that FGF20/FGF9 is sufficient for OHC and SC differentiation in the
288 basal turn of the cochlea at E13.5, in the middle and apical turns at E14.5-E15.5, and in the tip
289 of the apical turn at E15.5. Since the initiation of HC and SC differentiation occurs in the
290 base/mid-base of the cochlea at E13.5 and progresses apically over the next few days, these
291 results strongly imply that FGF20 functions during the initiation of differentiation, rather than
292 prosensory specification, consistent with our model (Fig 2D).
293
294 **Decrease in *Sox2* expression results in similar phenotypes as disruptions to**
295 **FGFR1 signaling**
296
297 Our results and previous findings suggest that FGFR1 regulates prosensory specification via
298 Sox2 [19]. Mice with an inner ear-specific *Sox2* hypomorphic mutation ($Sox2^{Ysb/Ysb}$, see below)
299 have defects in prosensory specification, accounting for a small loss of HCs and SCs, whereas
300 mice with inner-ear specific *Sox2* null mutations have a complete lack of prosensory
301 specification and a complete absence of sensory epithelium [12]. To examine how much the

302 reduction in *Sox2* expression in Fgfr1-CKO cochlea contributes to the phenotype at P0, we
303 combined the *Sox2*$^{-}$ (*Sox2* constitutive null) and *Sox2*^{Ysb} alleles to closely examine the effects of
304 reduction in *Sox2* expression on organ of Corti development, on a similar genetic background
305 as our Fgf20-KO and Fgfr1-CKO mice. We hypothesized that if *Fgfr1* acts upstream of *Sox2*,
306 then reducing *Sox2* expression should at least partially recapitulate the Fgfr1-CKO cochlea
307 phenotype. The *Sox2*^{Ysb} allele is a regulatory mutant in which transgene insertion in
308 chromosome 3 disrupts some otic enhancers, resulting in hypomorphic *Sox2* expression in the
309 inner ear [11,12].
310
311 We generated a *Sox2* allelic series of mice with the following genotypes, in order of highest to
312 lowest levels of *Sox2* expression: *Sox2*$^{+/+}$ (wildtype), *Sox2*$^{Ysb/+}$, *Sox2*$^{Ysb/Ysb}$, and *Sox2*$^{Ysb/-}$. In this
313 allelic series, decrease in *Sox2* expression had a dose-dependent effect on cochlea length at
314 P0 (Figs 4A-4C). *Sox2*$^{Ysb/+}$ cochleae had a 6% reduction in length compared to wildtype
315 (although not statistically significant), *Sox2*$^{Ysb/Ysb}$ cochleae had a 24% reduction, and *Sox2*$^{Ysb/-}$
316 had a 46% reduction. *Sox2*$^{Ysb/+}$ organ of Corti developed relatively normally, with three rows of
317 OHCs and one row of IHCs (Fig 4A). Interestingly, there were occasional ectopic IHCs medial
318 (neural) to the normal row of IHCs, especially in the middle and apical turns of the *Sox2*$^{Ysb/+}$
319 cochlea (Fig 4A, arrowheads). However, there was no significant increase in IHC number (total
320 or normalized to length) compared to wildtype cochleae (Fig 4D). The *Sox2*$^{Ysb/Ysb}$ cochlea
321 appeared much more abnormal, with gaps in the sensory epithelium that lacked HCs and SCs
322 in the basal turn (Figs 4A and 4B), similar to what was observed previously [12]. Moreover, at
323 the base, in the sensory islands between the gaps, there were often four rows of OHCs and six
324 rows of SCs. In the middle and apical turns, there were the normal three rows of OHCs and five
325 rows of SCs. There were also numerous ectopic IHCs throughout the middle and apical turns,
326 sometimes forming an entire second row of cells (Fig 4A), resulting in increased number of IHCs
327 in the middle turn compared to wildtype (S4A Fig). However, the total and length-normalized

328 number of IHCs in *Sox2*$^{Ysb/Ysb}$ cochleae did not significantly differ from that of wildtype cochleae
329 (Fig 4D). In terms of OHCs, *Sox2*$^{Ysb/Ysb}$ cochleae exhibited a 40% decrease in total number
330 compared to wildtype cochleae (Fig 4E). This decrease was not quite as severe when
331 normalized to cochlear length (21% decrease). Strikingly, *Sox2*$^{Ysb/-}$ cochleae lacked almost all
332 HCs and SCs, except in the apical turn (Figs 4A and 4B). The decrease in OHC number (93%)
333 in *Sox2*$^{Ysb/-}$ cochleae compared to wildtype was more severe than the decrease in IHC number
334 (75%). Notably, IHC number was significantly decreased in the basal and middle turns, but not
335 in the apical turn (S4A Fig). OHC number was significantly decreased throughout all three turns
336 (S4B Fig). In all of these genotypes, the number of SCs followed the pattern of loss of OHCs
337 (Fig 4F and S4C Fig). Interestingly, while *Sox2*$^{Ysb/-}$ cochleae almost completely lacked HCs and
338 SCs in the basal and middle turns, in 7 of 11 *Sox2*$^{Ysb/-}$ cochleae examined, one or two small
339 islands of HCs or SCs were found at the basal tip (S4D Fig).
340
341 Overall, these results showed that the basal end of the cochlea is more sensitive to the loss of
342 *Sox2* expression than the apical end. Furthermore, while both IHCs and OHCs were affected,
343 OHCs were more sensitive to decrease in *Sox2* expression than IHCs. Importantly, both of
344 these features were found in Fgfr1-CKO cochleae, where the decrease in IHCs was only found
345 in the basal and middle turns and there were almost no OHCs along the entire cochlear duct
346 (S1A and S1B Fig). Therefore, we conclude that decrease in *Sox2* expression, leading to
347 defects in prosensory specification, could account for the Fgfr1-CKO phenotype. Furthermore,
348 the decrease in *Sox2* expression could also account for the difference in severity between the
349 Fgf20-KO and Fgfr1-CKO phenotypes, since Fgf20-KO cochleae, which had normal *Sox2*
350 expression, did not have a decrease in the number of IHCs, unlike Fgfr1-CKO and *Sox2*$^{Ysb/-}$
351 cochleae.
352

353 **Decrease in levels of Sox2 expression delays prosensory specification**

354

355 We sought to determine why a decrease in *Sox2* expression more severely affected the basal
356 end of the cochlear duct. Initially, we examined *Sox2* expression at E14.5. As expected, Sox2
357 expression was almost completely absent in *Sox2*$^{Ysb/-}$ cochleae (S5A Fig). This decrease in
358 expression was not more severe at the basal turn of the cochlear duct, relative to the middle
359 and apical turns, suggesting that the more severe basal phenotype in *Sox2*$^{Ysb/-}$ cochleae cannot
360 be explained by differential Sox2 expression. Similarly, CDKN1B expression was downregulated
361 in the prosensory domain of *Sox2*$^{Ysb/-}$ cochleae, consistent with previous studies [12].
362 Interestingly, the decrease in expression was also not more severe at the basal turn relative to
363 the middle and apical turns (S5B Fig). Using CDKN1B as a marker of prosensory specification,
364 this suggests that the more severe basal phenotype also cannot be explained by differential
365 regulation of prosensory specification along the length of the cochlea.

366

367 As described in the introduction, waves of cell cycle exit (marking the completion of prosensory
368 specification) and initiation of differentiation travel in opposite directions along the cochlear duct
369 during development, resulting in the basal end of the cochlear duct differentiating immediately
370 after specification. The apical end, meanwhile, exhibits a delay in differentiation, resulting in a
371 longer temporal buffer between specification and differentiation. In this developmental pathway,
372 specification must be completed prior to the initiation of differentiation. We reasoned, therefore,
373 that disruptions to the timing of prosensory specification will preferentially interfere with basal
374 sensory epithelia development, potentially accounting for the more severe basal phenotype in
375 *Sox2* hypomorphs.

376

377 To test this hypothesis, we examined cell cycle exit in the prosensory domain via Ki67
378 expression, as a marker of the status of prosensory specification. Ki67 is expressed by cycling

379 cells, but not cells in G_0 [27]. In the developing cochlea at around E12.5 to E15.5, cells of the
380 prosensory domain, sometimes referred to as the zone of non-proliferation, have turned off or
381 are beginning to turn off Ki67 [3]. At E14.5 in *Sox2*$^{Ysb/+}$ cochleae, the prosensory domain along
382 most of the cochlear duct (serial sections 2-6) has turned off Ki67 expression, except at the very
383 base (serial section 1; Fig 5A, brackets). See graphical summary below Fig 5A; also see S5C
384 Fig for serial "mid-modiolar" sections through the cochlea. This indicates that the wave of cell
385 cycle exit, which starts at the apex, has reached the very base of the cochlear duct. However, in
386 *Sox2*$^{Ysb/-}$ cochleae, only the prosensory domain at the apical turn of the cochlear duct (serial
387 section 6) has turned off Ki67, not at the mid-basal or basal turns (serial sections 1-3); the
388 middle turns (serial sections 4 and 5), meanwhile, were just starting to turn off Ki67 (Fig 5A,
389 brackets). This indicates that cell cycle exit has only reached the middle turn, suggesting a
390 delay in prosensory specification. In addition, the nuclei of prosensory domain cells shift away
391 from the luminal surface of the cochlear epithelium upon specification [28]. This basal shift of
392 nuclei localization within the cell leaves a blank space between DAPI-stained nuclei and the
393 luminal surface of the cochlear duct, which can be visualized in all six serial sections in *Sox2*$^{Ysb/+}$
394 cochleae at E14.5 (Fig 5A, asterisks). However, in *Sox2*$^{Ysb/-}$ cochleae, cells of the prosensory
395 domain mostly did not exhibit this nuclei shift at E14.5.
396
397 At E15.5, the prosensory domain along the entire length of the cochlear duct has turned off Ki67
398 expression in both *Sox2*$^{Ysb/+}$ and *Sox2*$^{Ysb/-}$ cochleae (Fig 5A, brackets), indicating that
399 prosensory specification in *Sox2*$^{Ysb/-}$ cochleae has caught up by this stage. Prosensory nuclei
400 localization has also begun to catch up at E15.5 in *Sox2*$^{Ysb/-}$ cochleae (Fig 5A, asterisks).
401 Overall, these results suggest that prosensory specification is delayed in *Sox2*$^{Ysb/-}$ cochleae, but
402 not permanently disrupted.
403

404 By definition, prosensory specification must occur prior to differentiation to generate HCs and
405 SCs. Therefore, the period of time in between cell cycle exit and the initiation of differentiation
406 represents a temporal buffer (Fig 5B, green shading) preventing differentiation from initiating
407 prior to specification. As differentiation begins in the basal/mid-basal cochlear turns shortly after
408 specification, the delay in specification in *Sox2*$^{Ysb/-}$ cochleae leads to progenitors not having
409 been specified in time for differentiation at the basal end of the cochlear duct (Fig 5B,
410 crosshatch pattern). We propose that this at least partially explains why the basal end of the
411 cochlea is more sensitive to decreases in the level of *Sox2* expression. Moreover, since
412 differentiation begins in the mid-base and spreads to the rest of the base and apex, progenitors
413 at the basal tip in *Sox2*$^{Ysb/-}$ cochleae may still undergo specification prior to differentiation. This
414 may explain why small islands of HCs and SCs are sometimes seen in the basal tip of *Sox2*$^{Ysb/-}$
415 cochleae (S4D Fig).
416

417 ***Sox2* is upstream of *Fgf20***

418

419 While the delay in prosensory specification can explain the preferential loss of sensory
420 epithelium from the basal end of *Sox2* hypomorph cochleae, it does not readily explain the
421 preferential loss of OHCs, relative to IHCs. Since this preference for OHC loss is reminiscent of
422 the *Fgf20*/*Fgfr1* deletion phenotypes, we investigated the possibility that *Sox2* may be upstream
423 of FGF20-FGFR1 signaling. Interestingly, both *Etv4* and *Etv5* were dramatically downregulated
424 in the prosensory domain of *Sox2*$^{Ysb/-}$ cochleae compared to control (Fig 6A). This shows that
425 FGF20-FGFR1 signaling was disrupted in the *Sox2* hypomorph cochleae. Examination of *Fgfr1*
426 and *Fgf20* expression by in situ hybridization revealed that while *Fgfr1* expression did not
427 appear to be affected in *Sox2*$^{Ysb/-}$ cochleae at E14.5, *Fgf20* expression was absent (Fig 6B).
428 This suggests that while *Fgfr1* functions upstream of *Sox2*, *Fgf20* is downstream of *Sox2*. This

429 model predicts that *Fgf20* expression would be downregulated in Fgfr1-CKO cochleae, which
430 was confirmed by in situ hybridization (Fig 6C).
431
432 The above results indicate that the loss of *Fgf20* could partially account for the *Sox2*$^{Ysb/-}$
433 phenotype. To determine whether loss of *Fgf20* also causes delayed prosensory specification,
434 we examined Ki67 expression in Fgf20-KO cochleae. At E14.5, there was no detectable delay in
435 cell cycle exit in Fgf20-KO cochleae, as loss of Ki67 expression reached the base (serial section
436 1) in both control and Fgf20-KO cochleae (Fig 6D, brackets). See S6A Fig for serial "mid-
437 modiolar" sections through the cochlea. There was also no detectable delay in prosensory basal
438 nuclei shift in Fgf20-KO cochleae (Fig 6D, asterisks). These results were expected as the
439 Fgf20-KO phenotype is not more severe at the basal end of the cochlear duct. This is also
440 consistent with *Fgf20* being required during differentiation rather than prosensory specification
441 (Fig 2D). However, these results do not answer whether and how the loss of *Fgf20* contributes
442 to the *Sox2* hypomorph phenotype.
443
444 We also asked whether decrease in *Sox2* expression can account for the absence of
445 proliferation in Kölliker's organ of Fgfr1-CKO cochleae. Interestingly, EdU-incorporation was
446 decreased in Kölliker's organ in *Sox2*$^{Ysb/-}$ cochleae at E14.5, especially in the region adjacent to
447 the prosensory domain (S6B Fig, bracket). However, EdU-incorporation was not completely
448 absent from Kölliker's organ, unlike in Fgfr1-CKO cochleae. This suggests that loss of *Sox2* in
449 combination with other factors contributes to Kölliker's organ phenotype in Fgfr1-CKO cochleae.
450
451 **_Sox2_ and _Fgf20_ interact during cochlea development**
452
453 To explore how the loss of *Fgf20* contributes to the *Sox2* hypomorph phenotype, we combined
454 the *Fgf20*$^{-}$ and *Sox2*^{Ysb} alleles to generate *Fgf20* and *Sox2* compound mutants. We also

455 hypothesized that reducing *Sox2* expression in Fgf20-KO mice would recapitulate (or
456 phenocopy) the more severe Fgfr1-CKO phenotype. We interbred F1 mice from the same
457 parents to generate nine different F2 genotypes encompassing all possible combinations of the
458 *Fgf20*$^{-}$ and *Sox2*^{Ysb} alleles: *Fgf20*$^{+/+}$;*Sox2*$^{+/+}$, *Fgf20*$^{+/+}$;*Sox2*$^{Ysb/+}$, *Fgf20*$^{+/-}$;*Sox2*$^{+/+}$,
459 *Fgf20*$^{+/-}$;*Sox2*$^{Ysb/+}$, *Fgf20*$^{+/+}$;*Sox2*$^{Ysb/Ysb}$, *Fgf20*$^{+/-}$;*Sox2*$^{Ysb/Ysb}$, *Fgf20*$^{-/-}$;*Sox2*$^{+/+}$, *Fgf20*$^{-/-}$;*Sox2*$^{Ysb/+}$,
460 and *Fgf20*$^{-/-}$;*Sox2*$^{Ysb/Ysb}$ (Figs 7A and 7B and data not shown). At P0, an overview of HCs and
461 SCs showed that the *Fgf20*$^{+/-}$;*Sox2*$^{Ysb/+}$ phenotype mostly resembled that of *Fgf20*$^{+/+}$;*Sox2*$^{+/+}$,
462 *Fgf20*$^{+/+}$;*Sox2*$^{Ysb/+}$, and *Fgf20*$^{+/-}$;*Sox2*$^{+/+}$ cochleae, except for the prevalence of ectopic IHCs (Fig
463 7A, arrowheads). The *Fgf20*$^{+/-}$;*Sox2*$^{Ysb/Ysb}$ phenotype mostly resembled that of
464 *Fgf20*$^{+/+}$;*Sox2*$^{Ysb/Ysb}$ cochleae, but with more gaps in the basal cochlear turn and two rows of
465 IHCs throughout the length of the cochlear duct, except where there were gaps. The *Fgf20*$^{-}$
466 $^{/-}$;*Sox2*$^{Ysb/+}$ phenotype mostly resembled that of *Fgf20*$^{-/-}$;*Sox2*$^{+/+}$ cochleae, but with smaller
467 sensory islands in between gaps. The *Fgf20*$^{-/-}$;*Sox2*$^{Ysb/Ysb}$ phenotype appeared by far the most
468 severe, with almost a complete absence of IHCs, OHCs, and SCs from the basal turn, and tiny
469 sensory islands in the middle turn; however, the apical turn appeared similar to that of *Fgf20*$^{-}$
470 $^{/-}$;*Sox2*$^{Ysb/+}$ and *Fgf20*$^{-/-}$;*Sox2*$^{+/+}$ cochleae (Figs 7A and 7B).
471
472 Quantification of the phenotypes are presented in Figs 8B-8E and S7B-S7D Figs. We analyzed
473 the quantified P0 phenotype via two-way ANOVA with the two factors being gene dosage of
474 *Fgf20* (levels: *Fgf20*$^{+/+}$, *Fgf20*$^{+/-}$, *Fgf20*$^{-/-}$) and *Sox2* (levels: *Sox2*$^{+/+}$, *Sox2*$^{Ysb/+}$, *Sox2*$^{Ysb/Ysb}$).
475 Results from the two-way ANOVA and post-hoc Tukey's HSD are presented in Figs 8A, 8F, and
476 S7A and S8 Figs. Cochlear length and the total number of IHCs, OHCs, and SCs were all
477 significantly affected by both the *Fgf20* dosage and the *Sox2* dosage, as well as an interaction
478 between the two factors (Figs 8A-8E). The statistically significant interaction between *Fgf20* and
479 *Sox2* dosages suggests that *Fgf20* and *Sox2* have a genetic interaction in regulating cochlear
480 length as well as the number of IHCs, OHCs, and SCs (Fig 8A). Notably, *Fgf20*$^{+/-}$;*Sox2*$^{Ysb/Ysb}$

481 cochleae had significantly fewer OHCs and SCs than *Fgf20*$^{+/+}$;*Sox2*$^{Ysb/Ysb}$ cochleae, and *Fgf20*$^{-}$
482 $^{/-}$;*Sox2*$^{Ysb/+}$ cochleae had significantly fewer OHCs than *Fgf20*$^{-/-}$;*Sox2*$^{+/+}$ cochleae (Fig 8F).
483 Importantly, *Fgf20*$^{-/-}$;*Sox2*$^{Ysb/Ysb}$ cochleae had decreased total and length-normalized number of
484 IHCs, which was not observed in any of the other genotypes, strongly supporting a genetic
485 interaction between *Fgf20* and *Sox2* (*Fgf20*$^{+/+}$;*Sox2*$^{Ysb/Ysb}$ cochleae did have a slight decrease in
486 the total number IHCs, but not in the length-normalized number of IHCs).
487
488 Interestingly, while the total number of IHCs was decreased in *Fgf20*$^{-/-}$;*Sox2*$^{Ysb/Ysb}$ cochleae
489 relative to all other genotypes, this decrease was only found in the basal and middle turns, but
490 not the apical turn (S7B and S8 Figs). No such basal/middle/apical turn discrepancies existed in
491 the number of OHCs or SCs (S7C, S7D, and S8 Figs). This is reminiscent of the Fgfr1-CKO and
492 *Sox2*$^{Ysb/-}$ phenotypes.
493
494 To ensure that the *Fgf20*$^{-}$ and *Sox2*^{Ysb} interaction is not purely an artifact of the *Sox2*^{Ysb} allele,
495 we generated *Fgf20*$^{+/+}$;*Sox2*$^{+/+}$ (wildtype), *Fgf20*$^{+/-}$;*Sox2*$^{+/+}$ (Fgf20-het), *Fgf20*$^{+/+}$;*Sox2*$^{+/-}$ (Sox2-
496 het), and *Fgf20*$^{+/-}$;*Sox2*$^{+/-}$ (double het) mice to look for an interaction between the *Fgf20*$^{-}$ and
497 *Sox2*$^{-}$ alleles (S9A Fig). At P0, cochlear length did not significantly differ among the four
498 genotypes (S9B Fig). HC quantification showed that neither *Fgf20* nor *Sox2* exhibited
499 haploinsufficiency for total or length-normalized number of IHCs or OHCs (S9C and S9D Figs).
500 However, in Fgf20-het and much more so in Sox2-het cochleae, occasional ectopic IHCs can be
501 found in the middle and apical turns of the cochlear duct (S9A Fig, arrowheads). Interestingly, in
502 double het cochleae, many more ectopic IHCs were found, even in the basal turn. These
503 ectopic IHCs led to an increase in the total and length-normalized number of IHCs in double het
504 cochleae, compared to wildtype (S9C Fig). Notably, a significant increase in IHCs was only
505 found in the basal turn, not the middle or apical turns (S9E Fig). In the basal turn, IHC number
506 was significantly increased in double het cochleae compared to wildtype, Fgf20-het, and Sox2-

507 het cochleae. Double het cochleae also had a significant decrease in total and length-
508 normalized number of OHCs compared to wildtype (S9D Fig). Again, a significant decrease in
509 OHCs was only found in the basal turn, not the middle or apical turns (S9F Fig). These results
510 confirm a genetic interaction between *Fgf20* and *Sox2*.
511

512 **Loss of *Fgf20* does not further delay prosensory specification in *Sox2***
513 **hypomorph cochleae**
514

515 We propose that the *Fgf20*$^{-/-}$;*Sox2*$^{Ysb/Ysb}$ phenotype lies in between that of Fgfr1-CKO and
516 *Sox2*$^{Ysb/-}$ in terms of severity of reductions in cochlear length and in the number of HCs and
517 SCs. We further hypothesize that these three phenotypes form a continuum with the Fgf20-KO
518 phenotype (Fig 9A). Along this continuum, all four genotypes lack FGF20 signaling, but vary in
519 the level of *Sox2* expression and phenotype severity in the basal end of the cochlear duct and
520 the outer compartment (outer rows of OHCs and SCs). From this, and from the *Fgf20*$^{-}$ and
521 *Sox2*^{Ysb} series of alleles, we conclude that the basal end of the cochlear duct and the outer
522 compartment are more sensitive to the loss of *Fgf20* and *Sox2*, relative to the apical end and
523 inner compartment, respectively.
524

525 To determine the mechanism underlying the *Sox2* and *Fgf20* interaction, we asked whether the
526 similarity between the *Fgf20*$^{-/-}$;*Sox2*$^{Ysb/Ysb}$ and *Sox2*$^{Ysb/-}$ phenotypes could be explained by a
527 further decrease in *Sox2* levels in *Fgf20*$^{-/-}$;*Sox2*$^{Ysb/Ysb}$ cochleae from *Sox2*$^{Ysb/Ysb}$ levels. In other
528 words, we asked whether loss of *Fgf20* further reduces *Sox2* expression on a *Sox2*
529 hypomorphic background. Examination of prosensory domain *Sox2* expression at E14.5
530 revealed, as expected, that *Fgf20*$^{-/-}$;*Sox2*$^{Ysb/+}$ cochleae did not have a decrease in Sox2
531 expression compared to *Fgf20*$^{+/-}$;*Sox2*$^{Ysb/+}$ (S10A Fig). *Fgf20*$^{-/-}$;*Sox2*$^{Ysb/Ysb}$ cochleae also did not

532 have a further decrease in Sox2 expression compared to *Fgf20*$^{+/-}$;*Sox2*$^{Ysb/Ysb}$ cochleae.
533 Moreover, despite the loss of sensory epithelium in most of the basal turn, Sox2 expression was
534 not further decreased in the basal turn at E14.5 relative to the rest of the *Fgf20*$^{-/-}$;*Sox2*$^{Ysb/Ysb}$
535 cochlea (S10A Fig). These data confirm that *Fgf20* does not regulate *Sox2* expression. A similar
536 pattern of expression was observed for CDKN1B across the different genotypes (S10B Fig).
537 Loss of *Fgf20* did not contribute to a further decrease in CDKN1B expression on a *Sox2*$^{Ysb/Ysb}$
538 background, nor was there a basal-apical difference in CDKN1B expression in *Fgf20*$^{-}$
539 $^{/-}$;*Sox2*$^{Ysb/Ysb}$ cochleae at E14.5.
540
541 Next, we asked whether *Sox2* and *Fgf20* interact to delay prosensory specification. We showed
542 that Fgf20-KO cochleae do not exhibit a delay in prosensory specification (Fig 6D). However,
543 this does not rule out the possibility that the loss of *Fgf20* on a *Sox2* hypomorphic background
544 may contribute to a delay. We examined Ki67 expression at E14.5 and found that in
545 *Fgf20*$^{+/-}$;*Sox2*$^{Ysb/+}$ cochleae, prosensory domain cell cycle exit has reached the end of the base
546 (serial section 1; Fig 9B, brackets). See S10D Fig for serial “mid-modiolar” sections through the
547 cochlea. Similarly, cell cycle exit in *Fgf20*$^{-/-}$;*Sox2*$^{Ysb/+}$ cochleae also reached the very base. As
548 expected, *Fgf20*$^{+/-}$;*Sox2*$^{Ysb/Ysb}$ cochleae exhibited a slight delay in prosensory specification; cell
549 cycle exit has reached the base (serial section 2), but has not yet reached the end of the base
550 (serial section 1). Importantly, *Fgf20*$^{-/-}$;*Sox2*$^{Ysb/Ysb}$ cochleae did not show a further delay relative
551 to *Fgf20*$^{+/-}$;*Sox2*$^{Ysb/Ysb}$. There was also no detectable delay in basal nuclei shift in *Fgf20*$^{-}$
552 $^{/-}$;*Sox2*$^{Ysb/+}$ or *Fgf20*$^{-/-}$;*Sox2*$^{Ysb/Ysb}$ cochleae (Fig 9B, asterisks). These results suggest that the
553 loss of *Fgf20* does not contribute to delayed specification and that the severity of the *Fgf20*$^{-}$
554 $^{/-}$;*Sox2*$^{Ysb/Ysb}$ basal phenotype cannot be completely attributed to delayed specification.
555
556 Lastly, we examined proliferation in the *Fgf20*$^{-}$ and *Sox2*^{Ysb} E14.5 cochleae. Interestingly, there
557 was a noticeable decrease in the number of EdU-incorporating cells in Kölliker’s organ in *Fgf20*$^{-}$

558 $^{/-}$;*Sox2*$^{Ysb/Ysb}$ cochleae, compared to *Fgf20*$^{+/-}$;*Sox2*$^{Ysb/+}$, *Fgf20*$^{-/-}$;*Sox2*$^{Ysb/+}$, and *Fgf20*$^{+/-}$;*Sox2*$^{Ysb/Ysb}$
559 cochleae (S10C Fig). This phenotype is similar to that of *Sox2*$^{Ysb/-}$ cochleae and is less severe
560 than that of Fgfr1-CKO cochleae. This suggests that *Fgf20* and *Sox2* interact to regulate
561 proliferation in Kölliker's organ, although other factors downstream of *Fgfr1* also contribute.
562

563 **Fgf20-KO organ of Corti exhibits premature differentiation**

564

565 We showed that *Fgf20* likely plays a role during the initiation of differentiation. Previous studies
566 showed that deletion of both transcription factors *Hey1* and *Hey2* results in premature
567 differentiation in the organ of Corti [29]. Furthermore, it has been suggested that FGF signaling,
568 in particular FGF20, regulates *Hey1* and *Hey2* expression during this process [8,29]. To test
569 whether *Fgf20* is upstream of *Hey1* and *Hey2*, we looked at the expression of the two
570 transcription factors via in situ hybridization. In Fgf20-KO cochleae at E14.5, *Hey1* expression is
571 downregulated while *Hey2* is almost completely absent compared to control (Fig 10A). To test
572 whether FGF20 loss leads to premature differentiation, we examined myosin VI (Myo6)
573 expression, a marker of differentiated HCs [29]. At E14.5, the cochleae of 3 of 12 control
574 embryos examined contained Myo6-expressing HCs, while the cochleae of 18 of 19 littermate
575 Fgf20-KO embryos contained Myo6-expressing HCs ($p < 0.001$, Fisher's exact test; Fig 10B). If
576 present, the Myo6-expressing HCs at this stage were always found in the basal and mid-basal
577 turns of the cochlea. These results show that there is premature onset of differentiation in
578 Fgf20-KO cochleae, which begins in the basal/mid-basal turns. This result is surprising given
579 our previous finding of delayed differentiation in the apical end of Fgf20-KO cochleae at later
580 stages, which we confirm here (S1E Fig). These findings suggest that apical progression of
581 differentiation may be slower in Fgf20-KO cochleae.
582

583 Next, we asked whether ectopic activation of FGF signaling via overexpression of FGF9 will
584 delay the onset of differentiation. We generated Fgf20-het (*Fgf20*$^{Cre/+}$;*ROSA*$^{rtTA/+}$), Fgf20-null
585 (*Fgf20*$^{Cre/\beta gal}$;*ROSA*$^{rtTA/+}$), Fgf9-OA (*Fgf20*$^{Cre/+}$;*ROSA*$^{rtTA/+}$;TRE-Fgf9-IRES-eGfp), Fgf20-rescue
586 (*Fgf20*$^{Cre/\beta gal}$;*ROSA*$^{rtTA/+}$;TRE-Fgf9-IRES-eGfp) mice as before and started Dox induction at
587 E13.5 until E15.0 (Fig 3). At E15.0, all of the Fgf20-het (4/4) and Fgf20-null (4/4) cochleae
588 contained Myo6-expressing HCs, while none of the Fgf9-OA (0/4) and Fgf20-rescue (0/4)
589 cochleae contained Myo6-expressing HCs (Fig 10C). This suggests that ectopic expression of
590 FGF9 was able to delay the onset of differentiation, even with the lack of endogenous FGF20.
591 Despite this delay in onset of differentiation, by P0, differentiation has apparently caught up in
592 both Fgf9-OA and Fgf20-rescue cochleae (Fig 3A).
593
594 Similar to a delay in prosensory specification, premature onset of differentiation narrows the
595 temporal buffer between the completion of specification and initiation of differentiation towards
596 the cochlear base. In the context of a slight delay in specification due to decreased *Sox2* levels,
597 premature differentiation from the loss of *Fgf20* can lead to an attempt at differentiation before
598 specification in the basal end of the cochlea. We propose that *Sox2* and *Fgf20* interact to
599 regulate the boundaries of the temporal buffer, helping to ensure that differentiation begins after
600 the completion of specification (Fig 11).
601
602

603 ## Discussion

604

605 ### *Fgfr1* is involved in prosensory specification and differentiation, while *Fgf20* is
606 ### only involved in differentiation

607

608 *Fgf20* and *Fgfr1* are required for HC and SC development. Based on similarities in the
609 phenotype caused by the loss of FGF20 and loss of FGFR1 signaling, FGF20 has been
610 hypothesized as the FGFR1 ligand during organ of Corti development [17–21]. However, the
611 exact role of FGF20/FGFR1 during organ of Corti development has been a topic of debate. We
612 previously reported that Fgf20-KO mice do not have defects in prosensory specification, and
613 have a normally formed prosensory domain [21]. We further showed that FGF20 signaling is
614 important during the initiation stage of differentiation, and that Fgf20-KO cochleae have gaps in
615 the differentiated sensory epithelium filled with undifferentiated prosensory progenitors.
616 However, other studies have shown *in vitro* that FGF20 regulates prosensory specification via
617 Sox2 [33] and *in vivo* that FGFR1 is required for prosensory specification via Sox2 [19]. Here,
618 using an *in vivo* rescue model, we show that ectopic FGF9 signaling is sufficient to rescue the
619 Fgf20-KO phenotype in a spatiotemporal pattern that matched the timing of initiation of
620 differentiation along the length of the cochlear duct. We conclude, therefore, that FGF20 is
621 involved in differentiation and not necessary for prosensory specification.
622
623 Notably, the Fgf20-KO phenotype, in which two-thirds of OHCs fail to develop, is not as severe
624 as the Fgfr1-CKO phenotype, which lacks almost all OHCs as well as half of IHCs. Potential
625 explanations for this include differences in mouse genetic background, and the existence of a
626 redundant FGF ligand(s). To rule out the former, we examine here Fgf20-KO and Fgfr1-CKO
627 mice on a similar genetic background, and replicated the difference in phenotype severity. We
628 also replicated the decrease in *Sox2* expression in the prosensory domain previously reported
629 in Fgfr1-CKO mice [19]. We further reaffirmed that *Sox2* expression in the prosensory domain is
630 not affected by the loss of *Fgf20*. This suggests that another FGF ligand signaling through
631 FGFR1 is required to maintain *Sox2* expression during prosensory specification. The identity of
632 this ligand is currently unknown.
633

634 *Foxg1*^{Cre} has been used in several studies to target the otic epithelium, including to conditionally
635 delete *Fgfr1* [18–20]. One concern with *Foxg1*^{Cre} is that it is a null allele [22]. *Foxg1*-null mice
636 have shortened cochlear length, although HC and SC differentiation did not appear to be
637 directly affected [34]. Previous work [35] and our results here showed that *Foxg1* is not
638 haploinsufficient during cochlea development, as *Foxg1*$^{Cre/+}$;*Fgfr1*$^{flox/+}$ cochleae had very similar
639 phenotypes to *Fgfr1*$^{+/-}$ cochleae. Moreover, the use of the Six1enh21-Cre transgene, which
640 targets the otic epithelium in a similar spatiotemporal pattern as *Foxg1*^{Cre}, to conditionally delete
641 *Fgfr1* resulted in the same phenotype as *Foxg1*$^{Cre/+}$;*Fgfr1*$^{flox/-}$ cochleae [19]. This included the
642 loss of almost all OHCs, loss of IHCs, and decreased prosensory *Sox2* expression. Therefore,
643 the increased severity of *Foxg1*$^{Cre/+}$;*Fgfr1*$^{flox/-}$ cochleae relative to *Fgf20*$^{-/-}$ cochleae is likely not
644 attributable *Foxg1* haploinsufficiency.
645
646 We hypothesized that the severity of the Fgfr1-CKO phenotype is due to the loss of FGF20
647 signaling during differentiation and decreased *Sox2* expression causing disrupted prosensory
648 specification. Consistent with this hypothesis, the combination of *Fgf20*$^{-/-}$ and *Sox2*$^{Ysb/Ysb}$
649 mutations phenocopied Fgfr1-CKO cochleae. The similarities in phenotype include
650 approximately a 30% reduction in cochlear length and almost a complete loss of OHCs and SCs
651 and approximately a 50% loss of IHCs. Interestingly, the *Fgf20*$^{-/-}$;*Sox2*$^{Ysb/Ysb}$ phenotype is also
652 similar to the *Sox2*$^{Ysb/-}$ phenotype. We conclude that the Fgfr1-CKO, *Fgf20*$^{-/-}$;*Sox2*$^{Ysb/Ysb}$, and
653 *Sox2*$^{Ysb/-}$ phenotypes likely lie along the same continuum, as these three genotypes all exhibited
654 a lack of *Fgf20* expression or signaling and varying levels of *Sox2* expression (Fig 9A). Fgf20-
655 KO cochleae, in which *Sox2* expression was not affected, lies at the mild end of this continuum.
656 Interestingly, this continuum shows that in the absence of *Fgf20* expression or signaling,
657 reductions in the level of *Sox2* most severely affected sensory epithelium development of the
658 cochlear base and the outer compartment. Moving from the Fgf20-KO (mild) end of the

659 spectrum towards the *Sox2*$^{Ysb/-}$ (severe) end, increasing numbers of HCs and SCs are lost,
660 preferentially form the cochlear base and the outer compartment.
661
662 **_Sox2_ and _Fgf20_ interact to affect development towards the basal end of the**
663 **cochlea**
664
665 We show here conclusive evidence that *Sox2* and *Fgf20* genetically interact during cochlea
666 development. Interestingly, HC and SC development towards the basal end of the cochlea is
667 more severely affected by the loss of *Sox2* and *Fgf20* and their interaction. While we
668 hypothesize that *Sox2* and *Fgf20* are involved in distinct steps during organ of Corti
669 development (prosensory specification and differentiation, respectively), there is nevertheless
670 potential for a strong interaction. We propose that the timing of specification and differentiation
671 define a temporal buffer that normally prevents differentiation from initiating prior to the
672 completion of specification, and that *Sox2* and *Fgf20* modulate the borders of this buffer. In a
673 developmental pathway, the upstream event (specification) must occur prior to the downstream
674 event (differentiation). Therefore, loss of *Sox2* and *Fgf20* leading to delayed specification and
675 premature differentiation onset, respectively, disrupts the temporal buffer, especially towards the
676 cochlear base (Fig 11).
677
678 Specification must occur prior to the onset of differentiation. However, cell cycle exit does not
679 need to occur prior to the onset of differentiation, as mice lacking *Cdkn1b*, which is required for
680 cell cycle exit, still produce HCs and SCs (Chen & Segil, 1999; Kanzaki et al., 2006). Here, we
681 use cell cycle exit in the prosensory domain (also known as the zone of non-proliferation) as a
682 marker for the completion of specification (Chen & Segil, 1999). We hypothesize that
683 prosensory cells become specified and primed for differentiation upon withdrawal from the cell

684 cycle. Previous studies showed that prosensory cells are indeed capable of differentiating into
685 HCs and SCs directly after cell cycle exit, even in the apex. When *Shh* was deleted from the
686 spiral ganglion, differentiation began in the apex shortly after cell cycle exit and progressed
687 towards the base [5]. This suggests that specification occurs in an apex-to-base direction. We
688 cannot rule out, however, that specification occurs in the same direction as differentiation (base-
689 to-apex), independently of cell cycle exit. Such a scenario would still be consistent with our
690 model that a combination of delayed specification and premature onset of differentiation
691 accounts for the more severe basal phenotype in *Fgf20/Sox2* mutants.
692
693 The effect of loss of *Fgf20* on the timing of differentiation is small. We estimate that the onset of
694 differentiation in Fgf20-KO cochleae is advanced by only around 0.5 days. By itself, this effect
695 does not lead to a more severe mid-basal or basal phenotype in Fgf20-KO cochleae. However,
696 we present evidence that on a sensitized genetic background of delayed specification, this small
697 change in the timing of differentiation leads to a large defect in HC and SC production towards
698 the basal end of the cochleae. We propose that this at least partially explains the interaction
699 between *Sox2* and *Fgf20*. Furthermore, the relative sparing of development towards the apical
700 end of $Sox2^{Ysb/Ysb}$;$Fgf20^{-/-}$ cochleae, especially of IHCs, can be further explained by a delay in
701 differentiation at the apical end due to the loss of *Fgf20*. We do not know why an apical-basal
702 difference in timing of differentiation exists in Fgf20-KO cochleae. Perhaps there is a delay in
703 the apical progression of differentiation, or perhaps other factors contribute to the differentiation
704 of the apical end of the cochlea. Consistent with the latter, by P7 in Fgf20-KO cochleae, the
705 apical tip contains a full complement of IHCs and OHCs [21].
706
707 Notably, while we show the potential for a *Sox2* and *Fgf20* interaction in modulating the
708 temporal buffer between specification and differentiation, *Sox2* also has known roles during HC
709 and SC differentiation [13,15,37,38]. Therefore, the genetic interaction may occur during

710 differentiation as well. While interaction at this stage may explain the preferential loss of outer
711 compartment cells in *Sox2* and *Fgf20* mutants, it does not explain the selective loss of basal
712 cochlear HCs and SCs. Therefore, we conclude that the *Sox2* and *Fgf20* interaction regulates
713 the temporal buffer, with potential further interactions during differentiation.
714
715 The Notch ligand Jagged1 (Jag1) is thought to be important for cochlear prosensory
716 specification via lateral induction [39–45]. Interestingly, Notch signaling has also been shown to
717 be upstream of both *Fgf20* and *Sox2* in the developing cochlea [33]. Conditional deletion of
718 *Jag1* or *Rbpj*, the major transcriptional effector of canonical Notch signaling, resulted in the loss
719 of HCs and SCs, particularly from the basal end of the cochlear duct, similarly to *Fgf20*/*Sox2*
720 mutants. Unlike *Fgf20*/*Sox2* mutants, however, deletion of *Jag1* or *Rbpj* led to preferential loss
721 of Sox2 and CDKN1B expression from the prosensory domain at the basal end of the cochlea
722 [40,42,46]. This suggests that Jag1-Notch signaling is required for prosensory specification,
723 especially towards the cochlear base. This likely accounts for the more severe basal phenotype
724 of *Jag1* or *Rbpj* mutants. This same mechanism likely does not explain the more severe basal
725 phenotype of *Fgf20/Sox2* mutants, as Sox2 and CDKN1B expression was not more severely
726 reduced or absent in the cochlear base in these mice. Notably, not all studies agree that *Jag1* or
727 *Rbpj* is required for Sox2 and CDKN1B expression or for prosensory specification [47]. Further
728 studies are required to elucidate the functional relationship between *Jag1/Notch*, *Fgf20*, and
729 *Sox2* during cochlea development.
730
731 Other genes that potentially interact with *Fgf20* and *Sox2* during cochlea development include
732 *Mycn* (*N-Myc*) and *Mycl* (*L-Myc*). Interestingly, deletion of *Mycn* and *Mycl* from the cochlear
733 epithelium results in accelerated cell cycle exit and delayed initiation of differentiation [48],
734 opposite to the effects of loss of *Sox2* and *Fgf20*. Addressing potential interactions between
735 *Sox2*, *Fgf20*, *Mycn*, and *Mycl* is another topic for future studies.

736

737 **Outer compartment of the cochlear sensory epithelium is more sensitive to the**

738 **loss of *Fgfr1, Fgf20*, and *Sox2* than the inner compartment.**

739

740 In all of the genotypes we observed in this study, the loss of outer compartment cells (i.e.

741 OHCs) was predominant. Only in the most severe cases in which almost all OHCs were

742 missing, as seen in Fgfr1-CKO, *Fgf20*$^{-/-}$;*Sox2*$^{Ysb/Ysb}$, and *Sox2*$^{Ysb/-}$ cochleae, were IHCs also lost.

743 Similarly, reduction in SC number always preferentially affected the outermost cells. This

744 suggests that the organ of Corti outer compartment is more sensitive to the loss of *Fgfr1*, *Fgf20,*

745 and *Sox2* than the inner compartment. The combination of *Fgf20*$^{-}$ and *Sox2*^{Ysb} alleles elegantly

746 demonstrates this: as the number of *Fgf20*$^{-}$ and *Sox2*^{Ysb} alleles increased, the number of OHCs

747 progressively decreased. In the double homozygous mutants, the number of IHCs decreased as

748 well.

749

750 Previous studies noted that the dosage of *Fgfr1* affects the degree of organ of Corti outer

751 compartment loss. In *Fgfr1* hypomorphs with 80% reduction in transcription, only the third row of

752 OHCs were missing, while 90% hypomorphs had a slightly more severe phenotype [20].

753 Therefore, *Fgfr1* loss preferentially affects the outermost HCs. Other studies suggested that the

754 timing of *Fgfr1* deletion is important in determining the degree of outer compartment loss and

755 level of *Sox2* expression. When an earlier-expressed Cre driver (Six1enh21-Cre) was used to

756 conditionally delete *Fgfr1*, almost all OHCs and some IHCs were lost, with a 66% reduction in

757 *Sox2* expression at E14.5 [19]. When a later-expressed Cre driver (*Emx2*^{Cre}) was used, many

758 more OHCs and IHCs remained, with only a 12% reduction in *Sox2* expression. Our results are

759 consistent with both of these studies. We show that FGF20-independent FGFR1 signaling and

760 *Sox2* are required early, affecting both IHC and OHC development, while FGF20-FGFR1
761 signaling is important during later stages, affecting only OHC development.
762
763 Differentiation in the organ of Corti not only occurs in a basal-to-apical gradient, but also occurs
764 in an orthogonal inner-to-outer gradient. That is, IHCs differentiate first, followed by each
765 sequential row of OHCs [49]. This wave of differentiation suggests that perhaps outer
766 compartment HCs and SCs require a longer temporal buffer between specification and
767 differentiation. The genetic interaction between *Sox2* and *Fgf20* in modulating this temporal
768 buffer, therefore, could also account for the loss of outer compartment HCs and SCs. We
769 hypothesize that the requirement for a longer temporal buffer may also be involved in
770 determining OHC fate. In *Fgf20*$^{+/-}$;*Sox2*$^{+/-}$ cochleae, there was a slight decrease in OHCs that
771 was compensated for by ectopic IHCs, suggesting a fate switch from OHCs into IHCs. Here, we
772 confirmed previous suggestions that *Fgf20* regulates *Hey1* and *Hey2* to prevent premature
773 differentiation in the developing organ of Corti [8,29]. Interestingly, in *Hey1*/*Hey2* double
774 knockout cochleae, there was a similar slight decrease in OHCs compensated for by ectopic
775 IHCs [29]. Furthermore, inner ear-specific deletion of either *Smoothened* or *Neurod1*, which led
776 to premature differentiation in the apical cochlear turn, also led to loss of OHCs and the
777 presence of ectopic IHCs at the apex [6,8]. These findings further support a model where timing
778 of specification and differentiation affect IHC versus OHC fate, an interesting and important
779 topic for future studies.
780
781 Previously, we hypothesized that *Fgf20* is strictly required for the differentiation of an outer
782 compartment progenitor [21]. However, data we present here show that *Fgf20*, on a sensitized,
783 *Sox2* hypomorphic background, is also required for inner compartment differentiation. We
784 conclude that inner and outer compartment progenitors likely are not distinct populations.
785 Rather, all prosensory progenitors giving rise to the organ of Corti exist on an inner-to-outer

786 continuum. FGF20 signaling, in combination with other factors including Sox2, are required for
787 the proper development of all of these cells, though with varying sensitivities.
788

789 **The relationship between *Fgf20* and *Hey1/Hey2* in regulating differentiation is**
790 **complex**

791

792 We show *in vivo* that *Fgf20* is upstream of *Hey1* and *Hey2*. Supporting this result, *Fgfr1* has
793 also been shown *in vivo* to be upstream of *Hey2* [19]. Interestingly, in explant studies, inhibition
794 of FGF signaling alone did not result in decreased *Hey1/Hey2* expression or premature
795 differentiation [29]. However, FGF inhibition was able to rescue the overexpression of
796 *Hey1*/*Hey2* and the delay in differentiation induced by SHH signaling overactivation [8,29].
797 These discrepancies suggest that the relationship between *Fgf20* and *Hey1*/*Hey2* is more
798 complicated than we currently understand. Notably, *Hey1*/*Hey2* double knockout cochleae do
799 not exhibit a loss of OHCs to the extent of Fgf20-KO cochleae, suggesting that other genes
800 downstream of *Fgf20* are important in organ of Corti development. Moreover, deletion of *Fgf20*
801 only led to premature differentiation at the basal and mid-basal turns. *Fgf20* deletion actually
802 delayed differentiation in the apical end of the cochlea. Deletion of *Hey1*/*Hey2*, contrarily, led to
803 premature differentiation along the entire length of the cochlear duct, although it is unclear how
804 *Hey1/Hey2* loss affects the timing of apical differentiation beyond E15.0 [29]. This suggests that
805 other factors downstream of *Fgf20* interact with *Hey1*/*Hey2* to regulate the timing of
806 differentiation. Perhaps these same genes contribute to the loss of OHCs in Fgf20-KO
807 cochleae. *Mekk4*, which has been shown to be downstream of *Fgf20* and necessary for OHC
808 differentiation [50] could be one of these genes. Identifying other factors downstream of *Fgf20*
809 will be a topic of future studies.
810

811

812 # Materials and methods

813

814 ## Key Resources Table

Reagent type (species) or resource	Designation	Source or reference	Identifiers	Additional information
Genetic reagent (*M. musculus*)	*Fgf20*^{Cre}	Huh et al., 2015	MGI:5751785	
Genetic reagent (*M. musculus*)	*Fgf20*$^{\beta gal}$	Huh et al., 2012	RRID:MGI:5425887	
Genetic reagent (*M. musculus*)	*Foxg1*^{Cre}	Hébert and McConnell, 2000	RRID:IMSR_JAX:004337	
Genetic reagent (*M. musculus*)	*Fgfr1*^{flox}	Trokovic et al., 2003	RRID:IMSR_CMMR:0268	
Genetic reagent (*M. musculus*)	Sox2^{Cre}	Hayashi et al., 2002	RRID:IMSR_JAX:004783	
Genetic reagent (*M. musculus*)	*Sox2*^{Ysb}	Dong et al., 2002	RRID:IMSR_EM:05015	
Genetic reagent (*M. musculus*)	*Sox2*^{flox}	Shaham et al., 2009	RRID:IMSR_JAX:013093	
Genetic reagent (*M. musculus*)	*ROSA*^{rtTA}	Belteki et al., 2005	RRID:IMSR_JAX:005670	

Genetic reagent (*M. musculus*)	TRE-Fgf9-IRES-eGfp	White et al., 2006	MGI:5538516	
Recombinant DNA reagent	*pBluescriptKS-Fgfr1TM*	K. Peters		
Recombinant DNA reagent	*pGEMT-Fgf20*			
Recombinant DNA reagent	*pBluescriptSK-Sox2*	R. Lovell-Badge		Gift of A. Kiernan
Recombinant DNA reagent	*pGEM-Etv4*	G. Martin		
Recombinant DNA reagent	*pBluescriptSK-Etv5*	G. Martin		
Recombinant DNA reagent	*pT7T3D-Hey1*	IMAGE clone	#478014	Gift of S. Rentschler
Recombinant DNA reagent	*pCMVSPORT6-Hey2*	IMAGE clone	#5374813	Gift of S. Rentschler
Antibody	Sheep polyclonal anti-Digoxigenin-AP	Sigma-Aldrich	11093274910	1:1000
Antibody	Rabbit polyclonal anti-P75NTR	EMD Millipore	AB1554	1:300
Antibody	Rabbit polyclonal anti-Prox1	EMD Millipore	ABN278	1:1000
Antibody	Goat polyclonal anti-Sox2	Santa Cruz Biotechnology	sc-17320	1:200

Antibody	Rabbit polyclonal anti-p27Kip1	Neomarkers	RB-9019-P	1:50
Antibody	Rabbit polyclonal anti-Ki67	Abcam	ab15580	1:200
Antibody	Rabbit polyclonal anti-Myo6	Santa Cruz Biotechnology	sc-50461	1:100
Antibody	Donkey polyclonal anti-Rabbit IgG, Alexa Fluor 488	Thermo-Fisher Scientific	A-21206	1:500
Antibody	Donkey polyclonal anti-Goat IgG, Alexa Fluor 555	Thermo-Fisher Scientific	A-21432	1:500
Antibody	Goat polyclonal anti-Rabbit IgG, Flexa Fluor 555	Thermo-Fisher Scientific	A-21428	1:500
Chemical compound, drug	Alexa Fluor 488-conjugated Phalloidin	Invitrogen	A12379	1:50
Chemical compound, drug	Dox Diet, Grain-Based Doxycycline	Bio-Serv	S3888	
Chemical compound, drug	EdU (5-ethynyl-2'-deoxyuridine)	Thermo-Fisher Scientific	E10187	
Commercial assay or kit	Click-iT EdU Alexa Fluor 488 kit	Thermo-Fisher Scientific	C10337	

815

816 **Mice**

817

818 Mice were group housed with littermates, in breeding pairs, or in a breeding harem (2 females to
819 1 male), with food and water provided ad libitum.

820

821 For timed-pregnancy experiments, embryonic day 0.5 (E0.5) was assigned as noon of the day
822 the vaginal plug was found. For postnatal experiments, postnatal day 0 (P0) was determined as
823 the day of birth.

824

825 Mice were of mixed sexes and maintained on a mixed C57BL/6J x 129X1/SvJ genetic
826 background. All mice were backcrossed at least three generations onto this background. The
827 following mouse lines were used:

828 - *Fgf20*^{Cre} (*Fgf20*$^{-}$): knockin allele containing a sequence encoding a GFP-Cre fusion
829 protein replacing exon 1 of *Fgf20*, resulting in a null mutation [18].
830 - *Fgf20*$^{\beta gal}$: knockin allele containing a sequence encoding β-galactosidase (βgal)
831 replacing exon 1 of *Fgf20*, resulting in a null mutation [21].
832 - *Foxg1*^{Cre}: knockin allele containing a sequence encoding Cre fused in-frame downstream
833 of the first 13 codons, resulting in a null mutation [22].
834 - *Fgfr1*^{flox}: allele containing loxP sequences flanking exons 8 through 15 of *Fgfr1*. Upon
835 Cre-mediated recombination, produces a null mutation [51]
836 - *Fgfr1*$^{-}$: null allele generated by combining *Fgfr1*^{flox} with Sox2^{Cre} [52] to delete *Fgfr1* from
837 the epiblast.
838 - *ROSA*^{rtTA}: knockin allele containing a loxP-Stop-loxP sequence followed by a sequence
839 encoding rtTA-IRES-eGFP, targeted to the ubiquitously expressed *ROSA26* locus. Upon

840 Cre-mediated recombination, reverse tetracycline transactivator (rtTA) and eGFP are
841 expressed [25].
842 • TRE-Fgf9-IRES-eGfp: transgene containing seven tetracycline-inducible regulatory elements
843 driving the expression of FGF9-IRES-eGFP [26].
844 • *Sox2*^{Ysb}: Inner ear specific *Sox2* hypomorphic allele resulting from a random insertion of
845 a transgene in chromosome 3, likely interfering with tissue-specific *Sox2* regulatory
846 elements [11].
847 • *Sox2*$^{-}$: null allele generated by combining *Sox2*^{flox} [53] with Sox2^{Cre} to delete *Sox2* from
848 the epiblast.
849
850 All studies performed were in accordance with the Institutional Animal Care and Use Committee
851 at Washington University in St. Louis (protocol #20160113) and University of Nebraska Medical
852 Center (protocol #16-004-02 and 16-005-02).
853
854 **Doxycycline induction**
855
856 Pregnant dams were starved overnight the night before initiation of Dox induction and fed Dox
857 Diet, Grain-Based Doxycycline, 200 mg/kg (S3888, Bio-Serv, Flemington, NJ) ad libitum starting
858 at noon on the start date of Dox induction. On the stop date of Dox induction, Dox Diet was
859 replaced with regular mouse chow at noon.
860
861 **Sample preparation and sectioning**
862
863 For whole mount cochleae, inner ears were dissected out of P0 pups and fixed in 4% PFA in
864 PBS overnight at 4°C with gentle agitation. Samples were then washed x3 in PBS. Cochleae

865 were dissected away from the vestibule, otic capsule, and periotic mesenchyme with Dumont
866 #55 Forceps (RS-5010, Roboz, Gaithersburg, MD). The roof of the cochlear duct was opened
867 up by dissecting away the stria vascularis and Reissner's membrane; tectorial membrane was
868 removed to expose hair and supporting cells.
869
870 For sectioning, heads from E14.5 embryos were fixed in 4% PFA in PBS overnight at 4°C with
871 gentle agitation. Samples were then washed x3 in PBS and cryoprotected in 15% sucrose in
872 PBS overnight and then in 30% sucrose in PBS overnight. Samples were embedded in Tissue-
873 Tek O.C.T. compound (4583, VWR International, Radnor, PA) and frozen on dry ice. Serial
874 horizontal sections through base of the head were cut at 12 µm with a cryostat, dried at room
875 temperature, and stored at -80°C until use.
876
877 **RNA in situ hybridization**
878
879 Probe preparation: mouse cDNA plasmids containing the following inserts were used to make
880 RNA in situ probes, and were cut and transcribed with the indicated restriction enzyme (New
881 England Biolabs, Ipswich, MA) and RNA polymerase (New England Biolabs, Ipswich, MA):
882 *Fgfr1* transmembrane domain (325 bp, HincII, T7, gift of K. Peters), *Fgf20* (653 bp, NcoI, Sp6),
883 *Sox2* (750 bp, AccI, T3, gift of A. Kiernan), *Etv4* (~2300 bp, ApaI, Sp6, gift of G. Martin), *Etv5*
884 (~4000 bp, HindIII, T3, gift of G. Martin), *Hey1* (343 bp, EcoRI, T3, gift of S. Rentschler), *Hey2*
885 (819 bp, EcoRI, T7, gift of S. Rentschler). Restriction digest and *in vitro* transcription were done
886 according to manufacturer's instructions, with DIG RNA Labeling Mix (11277073910, Sigma-
887 Aldrich, St. Louis, MO). After treatment with RNase-free DNase I (04716728001, Sigma-Aldrich,
888 St. Louis, MO) for 15 min at 37°C, probes were hydrolyzed in hydrolysis buffer (40 mM
889 $NaHCO_3$, 60 mM Na_2CO_3) at 60°C for up to 30 min, depending on probe size.
890

891 Frozen section in situ hybridization: frozen slides were warmed for 20 min at room temperature
892 and then 5 min at 50°C on a slide warmer. Sections were fixed in 4% PFA in PBS for 20 min at
893 room temperature, washed x2 in PBS and treated with pre-warmed 10 µg/ml Proteinase K
894 (03115828001, Sigma-Aldrich, St. Louis, MO) in PBS for 7 min at 37°C. Sections were then
895 fixed in 4% PFA in PBS for 15 min at room temperature, washed x2 in PBS, acetylated in 0.25%
896 acetic anhydrate in 0.1M Triethanolamine, pH 8.0, for 10 min, and washed again in PBS.
897 Sections were then placed in pre-warmed hybridization buffer (50% formamide, 5x SSC buffer,
898 5 mM EDTA, 50 µg/ml yeast tRNA) for 3 h at 60°C in humidified chamber for prehybridization.
899 Sections were then hybridized in 10 µg/ml probe/hybridization buffer overnight (12-16 h) at
900 60°C. The next day, sections were washed in 1x SSC for 10 min at 60°C, followed by 1.5x SSC
901 for 10 min at 60°C, 2x SSC for 20 min at 37°C x2, and 0.2x SSC for 30 min at 60°C x2. Sections
902 were then washed in KTBT (0.1 M Tris, pH 7.5, 0.15 M NaCl, 5 mM KCl, 0.1% Triton X-100) at
903 room temperature and blocked in KTBT + 20% sheep serum + 2% Blocking Reagent
904 (11096176001, Sigma-Aldrich, St. Louis, MO) for 4 h. Blocking Reagent was dissolved in 100
905 mM Maleic acid, 150 mM NaCl, pH 7.5. Sections were then incubated in sheep anti-
906 Digoxigenin-AP, Fab fragments (1:1000, 11093274910, Sigma-Aldrich, St. Louis, MO) in KTBT
907 + 20% sheep serum + 2% Blocking Reagent overnight at 4°C. Sections were then washed x3 in
908 KTBT for 30 min at room temperature, and then washed x2 in NTMT (0.1 M Tris, pH 9.5, 0.1 M
909 NaCl, 50 mM $MgCl_2$, 0.1% Tween 20) for 15 min. Sections were next incubated in NTMT +
910 1:200 NBT/BCIP Stock Solution (11681451001, Sigma-Aldrich, St. Louis, MO) in the dark at
911 room temperature until color appeared. Sections were then washed in PBS, post-fixed in 4%
912 PFA in PBS for 15 min and washed x2 in PBS. Finally, sections were dehydrated in 30% and
913 then 70% methanol, 5 min each, followed by 100% methanol for 15 min. Sections were then
914 rehydrated in 70% and 30% methanol and then PBS, 5 min each, and mounted in 95% glycerol.
915

916 **Immunofluorescence**

917

918 Whole mount: cochleae were incubated in PBS + 0.5% Tween-20 (PBSTw) for 1 h to
919 permeabilize. Cochleae were then blocked using PBSTw + 5% donkey serum for 1 h and then
920 incubated in PBSTw + 1% donkey serum with the primary antibody overnight at 4°C. Cochleae
921 were then washed x3 in PBS and incubated in PBS + 1% Tween-20 with the secondary
922 antibody. After wash in PBS x3, cochleae were mounted in 95% glycerol with the sensory
923 epithelium facing up.

924

925 Frozen slides were warmed for 30 min at room temperature and washed in PBS before
926 incubating in PBS + 0.5% Triton X-100 (PBST) for 1 h to permeabilize the tissue. Sections were
927 then blocked using in PBST + 5% donkey serum for 1 h and then incubated in PBST + 1%
928 donkey serum with the primary antibody overnight at 4°C in a humidified chamber. Sections
929 were then washed x3 in PBS and incubated in PBS + 1% Triton X-100 with the secondary
930 antibody. After wash in PBS x3, slides were mounted in VectaShield antifade mounting medium
931 with DAPI (H-1200, Vector Labs, Burlingame, CA).

932

933 **Cell proliferation assay**

934

935 EdU (E10187, Thermo-Fisher Scientific, Waltham, MA) was injected i.p. into pregnant dams at
936 100 µg per gram body weight. Embryos were harvested at 1 h after injection. EdU was detected
937 using the Click-iT EdU Alexa Fluor 488 kit (C10337, Thermo-Fisher Scientific, Waltham, MA)
938 according to manufacturer's instructions.

939

940 **Imaging**

941

942 Brightfield microscopy was done using a Hamamatsu NanoZoomer slide scanning system with
943 a 20x objective. Images were processed with the NanoZoomer Digital Pathology (NDP.view2)
944 software.

945

946 Fluorescent microscopy was done using a Zeiss LSM 700 confocal or Zeiss Axio Imager Z1 with
947 Apotome 2, with z-stack step-size determined based on objective lens type (10x or 20x), as
948 recommended by the ZEN software (around 1 μm). Fluorescent images shown are maximum
949 projections. Low magnification fluorescent images shown of the whole cochlear duct required
950 stitching together, by hand, several images. Images were processed with ImageJ
951 (imagej.nih.gov).

952

953 **Quantification**

954

955 Measurements and cell quantification (using the Cell Counter plugin by Kurt De Vos) were done
956 using ImageJ. Total cochlear duct length was defined as the length from the very base of the
957 cochlea to the very tip of the apex, along the tunnel of Corti. Hair cells were identified via
958 Phalloidin, which binds to F-actin [54]. Inner pillar cells were labeled via p75NTR [55], and
959 supporting cells (SCs, including pillar cells and Deiters' cells) were labeled with a combination of
960 Prox1 [56] and Sox2 [10]. Inner hair cells (IHCs) were differentiated from outer hair cells (OHCs)
961 based on their neural/abneural location, respectively, relative to p75NTR-expressing inner pillar
962 cells. For total cell counts, IHCs, OHCs, and SCs were counted along the entire length of the
963 cochlea. Total cell counts were also normalized to cochlear length and presented as cell count
964 per 100 μm of cochlea (e.g. IHCs/100 μm). For cell quantification at the basal, middle, and

965 apical turns of the cochlea, the cochlear duct was evenly divided into thirds, and total IHCs,
966 OHCs, and SCs were quantified for each third and normalized to length. For the Fgf20-rescue
967 experiments in Fig 3, IHCs, OHCs, and SCs from at least 300 μm regions of the basal (10%),
968 middle (40%), and apical (70%) turns of the cochleae were counted and normalized to 100 μm
969 along the length of the cochlear duct.
970
971 In Sox2$^{Ysb/-}$ cochleae, p75NTR expression was mostly absent, resulting in sensory islands
972 without p75NTR-expressing inner pillar cells. In these cochleae, HCs not associated with inner
973 pillar cells were presumed to be IHCs during quantification. When a curved line was drawn
974 connecting the p75NTR islands along the organ of Corti, these presumed IHCs were always
975 medial (neural) to that line.
976
977 **Statistical analysis and plotting**
978
979 All figures were made in Canvas X (ACD systems). Data analysis was performed using the
980 Python programming language (python.org) in Jupyter Notebook (jupyter.org) with the following
981 libraries: Pandas (pandas.pydata.org), NumPy (numpy.org) and SciPy (scipy.org). Plotting was
982 done using the Matplotlib library (matplotlib.org). Statistics (t-test, one-way ANOVA, two-way
983 ANOVA, and Fisher's exact test) were performed using the SciPy module Stats; Tukey's HSD
984 was performed using the Statsmodels package (statsmodels.org). All comparisons of two
985 means were performed using two-tailed, unpaired Student's t-test. For comparisons of more
986 than two means, one-way ANOVA was used, except in Fig 8 and S7 Fig, where two-way
987 ANOVA was used, with the factors being *Fgf20* (levels: *Fgf20*$^{+/+}$, *Fgf20*$^{+/-}$, *Fgf20*$^{-/-}$) and *Sox2*
988 (levels: *Sox2*$^{+/+}$, *Sox2*$^{Ysb/+}$, *Sox2*$^{Ysb/Ysb}$) gene dosage. For significant ANOVA results at $\alpha = 0.05$,
989 Tukey's HSD was performed for post-hoc pair-wise analysis. In all cases, $p < 0.05$ was
990 considered statistically significant. All statistical details can be found in the figures and figure

991 legends. In all cases, each sample (each data point in graphs) represents one animal. Based on
992 similar previous studies, a sample size of 3-5 was determined to be appropriate. Error bars
993 represent mean ± standard deviation (SD). For qualitative comparisons (comparing expression
994 via immunofluorescence or RNA in situ hybridization), at least three samples were examined
995 per genotype. All images shown are representative.
996
997 Evaluation of onset of Myo6-expressing cells (Figs 10B and 10C): 3 or 4 serial sections through
998 the entire cochleae were immunostained for Myo6 and evaluated, blinded to genotype, for the
999 presence of Myo6-expressing cells. E14.5 embryos were further stage-matched based on
1000 interdigital webbing of the hindlimb (at E14.5, roughly half of the hindlimb interdigital webbing is
1001 still present). Of the 34 embryos at E14.5, 3 were removed from analysis due to lack of or
1002 minimal hindlimb interdigital webbing (too old relative to the other embryos).
1003

1004 ## Acknowledgements

1005 We would like to thank Drew Hagan, Kel Vin Woo, and Yongjun Yin for their critical reading of
1006 the manuscript.
1007

1008 ## References

1009

1010 1. Basch ML, Brown RM, Jen H-I, Groves AK. Where hearing starts: the development of the
1011 mammalian cochlea. J Anat. 2016 Feb;228(2):233–54.

1012 2. Fekete DM, Muthukumar S, Karagogeos D. Hair Cells and Supporting Cells Share a
1013 Common Progenitor in the Avian Inner Ear. J Neurosci. 1998 Oct 1;18(19):7811–21.

1014 3. Chen P, Segil N. p27(Kip1) links cell proliferation to morphogenesis in the developing
1015 organ of Corti. Development. 1999 Apr;126(8):1581–90.

1016 4. Lee Y-S, Liu F, Segil N. A morphogenetic wave of p27Kip1 transcription directs cell cycle
1017 exit during organ of Corti development. Development. 2006 Aug 1;133(15):2817–26.

1018 5. Bok J, Zenczak C, Hwang CH, Wu DK. Auditory ganglion source of Sonic hedgehog
1019 regulates timing of cell cycle exit and differentiation of mammalian cochlear hair cells. Proc
1020 Natl Acad Sci U S A. 2013 Aug 20;110(34):13869–74.

1021 6. Jahan I, Pan N, Kersigo J, Fritzsch B. Neurod1 Suppresses Hair Cell Differentiation in Ear
1022 Ganglia and Regulates Hair Cell Subtype Development in the Cochlea. Riley B, editor.
1023 PLOS ONE. 2010 Jul 22;5(7):e11661.

1024 7. Matei V, Pauley S, Kaing S, Rowitch D, Beisel K w., Morris K, et al. Smaller inner ear
1025 sensory epithelia in Neurog1 null mice are related to earlier hair cell cycle exit. Dev Dyn.
1026 2005 Nov 1;234(3):633–50.

1027 8. Tateya T, Imayoshi I, Tateya I, Hamaguchi K, Torii H, Ito J, et al. Hedgehog signaling
1028 regulates prosensory cell properties during the basal-to-apical wave of hair cell
1029 differentiation in the mammalian cochlea. Development. 2013 Sep 15;140(18):3848–57.

1030 9. Gu R, Brown RM, Hsu C-W, Cai T, Crowder AL, Piazza VG, et al. Lineage tracing of Sox2-
1031 expressing progenitor cells in the mouse inner ear reveals a broad contribution to non-
1032 sensory tissues and insights into the origin of the organ of Corti. Dev Biol. 2016
1033 01;414(1):72–84.

1034 10. Mak ACY, Szeto IYY, Fritzsch B, Cheah KSE. Differential and overlapping expression
1035 pattern of SOX2 and SOX9 in inner ear development. Gene Expr Patterns. 2009 Sep
1036 1;9(6):444–53.

1037 11. Dong S, Leung KKH, Pelling AL, Lee PYT, Tang ASP, Heng HHQ, et al. Circling,
1038 Deafness, and Yellow Coat Displayed by Yellow Submarine (Ysb) and Light Coat and
1039 Circling (Lcc) Mice with Mutations on Chromosome 3. Genomics. 2002 Jun;79(6):777–84.

1040 12. Kiernan AE, Pelling AL, Leung KKH, Tang ASP, Bell DM, Tease C, et al. Sox2 is required
1041 for sensory organ development in the mammalian inner ear. Nature. 2005 Apr
1042 21;434(7036):1031–5.

1043 13. Dabdoub A, Puligilla C, Jones JM, Fritzsch B, Cheah KSE, Pevny LH, et al. Sox2 signaling
1044 in prosensory domain specification and subsequent hair cell differentiation in the
1045 developing cochlea. Proc Natl Acad Sci U S A. 2008 Nov 25;105(47):18396–401.

1046 14. Pan W, Jin Y, Chen J, Rottier RJ, Steel KP, Kiernan AE. Ectopic Expression of Activated
1047 Notch or SOX2 Reveals Similar and Unique Roles in the Development of the Sensory Cell
1048 Progenitors in the Mammalian Inner Ear. J Neurosci. 2013 Oct 9;33(41):16146–57.

1049 15. Puligilla C, Kelley MW. Dual role for Sox2 in specification of sensory competence and
1050 regulation of Atoh1 function. Dev Neurobiol. 2016;77(1):3–13.

1051 16. Ebeid M, Huh S-H. FGF signaling: diverse roles during cochlear development. BMB Rep.
1052 2017 Oct 31;50(10):487–95.

1053 17. Hayashi T, Ray CA, Bermingham-McDonogh O. Fgf20 Is Required for Sensory Epithelial
1054 Specification in the Developing Cochlea. J Neurosci. 2008 Jun 4;28(23):5991–9.

1055 18. Huh S-H, Warchol ME, Ornitz DM. Cochlear progenitor number is controlled through
1056 mesenchymal FGF receptor signaling. eLife. 2015 Apr 27;4:e05921.

1057 19. Ono K, Kita T, Sato S, O'Neill P, Mak S-S, Paschaki M, et al. FGFR1-Frs2/3 Signalling
1058 Maintains Sensory Progenitors during Inner Ear Hair Cell Formation. Cheah KSE, editor.
1059 PLOS Genet. 2014 Jan 23;10(1):e1004118.

1060 20. Pirvola U, Ylikoski J, Trokovic R, Hébert JM, McConnell SK, Partanen J. FGFR1 is
1061 required for the development of the auditory sensory epithelium. Neuron. 2002 Aug
1062 15;35(4):671–80.

1063 21. Huh S-H, Jones J, Warchol ME, Ornitz DM. Differentiation of the Lateral Compartment of
1064 the Cochlea Requires a Temporally Restricted FGF20 Signal. Groves A, editor. PLOS Biol.
1065 2012 Jan 3;10(1):e1001231.

1066 22. Hébert JM, McConnell SK. Targeting of cre to the Foxg1 (BF-1) Locus Mediates loxP
1067 Recombination in the Telencephalon and Other Developing Head Structures. Dev Biol.
1068 2000 Jun 15;222(2):296–306.

1069 23. Ornitz DM, Itoh N. The Fibroblast Growth Factor signaling pathway. Wiley Interdiscip Rev
1070 Dev Biol. 2015 May 1;4(3):215–66.

1071 24. Zhang X, Ibrahimi OA, Olsen SK, Umemori H, Mohammadi M, Ornitz DM. Receptor
1072 Specificity of the Fibroblast Growth Factor Family: THE COMPLETE MAMMALIAN FGF
1073 FAMILY. J Biol Chem. 2006 Jun 9;281(23):15694–700.

1074 25. Belteki G, Haigh J, Kabacs N, Haigh K, Sison K, Costantini F, et al. Conditional and
1075 inducible transgene expression in mice through the combinatorial use of Cre-mediated
1076 recombination and tetracycline induction. Nucleic Acids Res. 2005 Jan 1;33(5):e51–e51.

1077 26. White AC, Xu J, Yin Y, Smith C, Schmid G, Ornitz DM. FGF9 and SHH signaling
1078 coordinate lung growth and development through regulation of distinct mesenchymal
1079 domains. Development. 2006 Apr 15;133(8):1507–17.

1080 27. Scholzen T, Gerdes J. The Ki-67 protein: From the known and the unknown. J Cell
1081 Physiol. 2000 Mar 1;182(3):311–22.

1082 28. Kelley MW. Cellular commitment and differentiation in the organ of Corti. Int J Dev Biol.
1083 2007;51(6–7):571–83.

1084 29. Benito-Gonzalez A, Doetzlhofer A. Hey1 and Hey2 Control the Spatial and Temporal
1085 Pattern of Mammalian Auditory Hair Cell Differentiation Downstream of Hedgehog
1086 Signaling. J Neurosci. 2014 Sep 17;34(38):12865–76.

1087 30. Bermingham NA, Hassan BA, Price SD, Vollrath MA, Ben-Arie N, Eatock RA, et al. Math1:
1088 an essential gene for the generation of inner ear hair cells. Science. 1999 Jun
1089 11;284(5421):1837–41.

1090 31. Cai T, Seymour ML, Zhang H, Pereira FA, Groves AK. Conditional Deletion of Atoh1
1091 Reveals Distinct Critical Periods for Survival and Function of Hair Cells in the Organ of
1092 Corti. J Neurosci. 2013 Jun 12;33(24):10110–22.

1093 32. Woods C, Montcouquiol M, Kelley MW. Math1 regulates development of the sensory
1094 epithelium in the mammalian cochlea. Nat Neurosci. 2004 Dec;7(12):1310–8.

1095 33. Munnamalai V, Hayashi T, Bermingham-McDonogh O. Notch Prosensory Effects in the
1096 Mammalian Cochlea Are Partially Mediated by Fgf20. J Neurosci. 2012 Sep
1097 12;32(37):12876–84.

1098 34. Pauley S, Lai E, Fritzsch B. Foxg1 is required for morphogenesis and histogenesis of the
1099 mammalian inner ear. Dev Dyn. 2006 Sep;235(9):2470–82.

1100 35. Brown AS, Epstein DJ. Otic ablation of smoothened reveals direct and indirect
1101 requirements for Hedgehog signaling in inner ear development. Development. 2011 Sep
1102 15;138(18):3967–76.

1103 36. Kanzaki S, Beyer LA, Swiderski DL, Izumikawa M, Stöver T, Kawamoto K, et al. p27Kip1
1104 deficiency causes organ of Corti pathology and hearing loss. Hear Res. 2006 Apr
1105 1;214(1):28–36.

1106 37. Ahmed M, Wong EYM, Sun J, Xu J, Wang F, Xu P-X. Eya1-Six1 Interaction Is Sufficient to
1107 Induce Hair Cell Fate in the Cochlea by Activating Atoh1 Expression in Cooperation with
1108 Sox2. Dev Cell. 2012 Feb;22(2):377–90.

1109 38. Kempfle JS, Turban JL, Edge ASB. Sox2 in the differentiation of cochlear progenitor cells.
1110 Sci Rep. 2016;6:23293.

1111 39. Bosman EA, Quint E, Fuchs H, Hrabé de Angelis M, Steel KP. Catweasel mice: a novel
1112 role for Six1 in sensory patch development and a model for branchio-oto-renal syndrome.
1113 Dev Biol. 2009 Apr 15;328(2):285–96.

1114 40. Brooker R. Notch ligands with contrasting functions: Jagged1 and Delta1 in the mouse
1115 inner ear. Development. 2006 Apr 1;133(7):1277–86.

1116 41. Kiernan AE, Ahituv N, Fuchs H, Balling R, Avraham KB, Steel KP, et al. The Notch ligand
1117 Jagged1 is required for inner ear sensory development. Proc Natl Acad Sci U S A.
1118 2001;98(7):3873–3878.

1119 42. Kiernan AE, Xu J, Gridley T. The Notch ligand JAG1 is required for sensory progenitor
1120 development in the mammalian inner ear. PLOS Genet. 2006;2(1):e4.

1121 43. Kiernan AE, Li R, Hawes NL, Churchill GA, Gridley T. Genetic background modifies inner
1122 ear and eye phenotypes of jag1 heterozygous mice. Genetics. 2007 Sep;177(1):307–11.

1123 44. Moayedi Y, Basch ML, Pacheco NL, Gao SS, Wang R, Harrison W, et al. The Candidate
1124 Splicing Factor Sfswap Regulates Growth and Patterning of Inner Ear Sensory Organs.
1125 Wu DK, editor. PLOS Genet. 2014 Jan 2;10(1):e1004055.

1126 45. Tsai H, Hardisty RE, Rhodes C, Kiernan AE, Roby P, Tymowska-Lalanne Z, et al. The
1127 mouse slalom mutant demonstrates a role for Jagged1 in neuroepithelial patterning in the
1128 organ of Corti. Hum Mol Genet. 2001 Mar 1;10(5):507–12.

1129 46. Yamamoto N, Chang W, Kelley MW. Rbpj regulates development of prosensory cells in the
1130 mammalian inner ear. Dev Biol. 2011 May;353(2):367–79.

1131 47. Basch ML, Ohyama T, Segil N, Groves AK. Canonical Notch Signaling Is Not Necessary
1132 for Prosensory Induction in the Mouse Cochlea: Insights from a Conditional Mutant of
1133 RBPj. J Neurosci. 2011 Jun 1;31(22):8046–58.

1134 48. Kopecky BJ, Jahan I, Fritzsch B. Correct Timing of Proliferation and Differentiation is
1135 Necessary for Normal Inner Ear Development and Auditory Hair Cell Viability: Mycs' Role
1136 in Ear Development. Dev Dyn. 2013 Feb;242(2):132–47.

1137 49. Chen P, Johnson JE, Zoghbi HY, Segil N. The role of Math1 in inner ear development:
1138 Uncoupling the establishment of the sensory primordium from hair cell fate determination.
1139 Development. 2002 May;129(10):2495–505.

1140 50. Haque K, Pandey AK, Zheng H-W, Riazuddin S, Sha S-H, Puligilla C. MEKK4 Signaling
1141 Regulates Sensory Cell Development and Function in the Mouse Inner Ear. J Neurosci.
1142 2016 Jan 27;36(4):1347–61.

1143 51. Trokovic N, Trokovic R, Mai P, Partanen J. Fgfr1 regulates patterning of the pharyngeal
1144 region. Genes Dev. 2003 Jan 1;17(1):141–53.

1145 52. Hayashi S, Lewis P, Pevny L, McMahon AP. Efficient gene modulation in mouse epiblast
1146 using a Sox2Cre transgenic mouse strain. Mech Dev. 2002 Dec;119 Suppl 1:S97–101.

1147 53. Shaham O, Smith AN, Robinson ML, Taketo MM, Lang RA, Ashery-Padan R. Pax6 is
1148 essential for lens fiber cell differentiation. Development. 2009 Aug 1;136(15):2567–78.

1149 54. Avinash GB, Nuttall AL, Raphael Y. 3-D analysis of F-actin in stereocilia of cochlear hair
1150 cells after loud noise exposure. Hear Res. 1993 May 1;67(1):139–46.

1151 55. Mueller KL, Jacques BE, Kelley MW. Fibroblast Growth Factor Signaling Regulates Pillar
1152 Cell Development in the Organ of Corti. J Neurosci. 2002 Nov 1;22(21):9368–77.

1153 56. Bermingham-McDonogh O, Oesterle EC, Stone JS, Hume CR, Huynh HM, Hayashi T.
1154 Expression of Prox1 during mouse cochlear development. J Comp Neurol. 2006 May
1155 10;496(2):172–86.

1156

1157 **Figure titles and legends**

1158

1159 **Fig 1. The Fgf20-KO cochlear phenotype is less severe than the Fgfr1-CKO**

1160 **phenotype**

1161 (A, B) Whole mount cochlea from P0 *Fgf20*$^{+/-}$, *Fgf20*$^{-/-}$, *Foxg1*$^{Cre/+}$;*Fgfr1*$^{flox/+}$, and

1162 *Foxg1*$^{Cre/+}$;*Fgfr1*$^{flox/-}$ mice showing (A) inner and outer hair cells (IHC and OHC,

1163 phalloidin, green) separated by inner pillar cells (p75NTR, red) and (B) supporting cells

1164 (Prox1 and Sox2, green/yellow). Magnifications show the basal, middle, and apical turns

1165 of the cochlea. Scale bar, 100 μm (magnifications), 1 mm (whole).

1166 (C-F) Quantification of (C) cochlear duct length, (D) total IHCs and IHCs per 100 μm of the

1167 cochlear duct, (E) total OHCs and OHCs per 100 μm, and (F) total supporting cells

1168 (SCs) and SCs per 100 μm at P0. *Fgf20*$^{+/-}$ and *Fgf20*$^{-/-}$ cochleae results were analyzed

1169 by unpaired Student's t test; *Fgfr1*$^{flox/+}$, *Fgfr1*$^{flox/-}$, *Foxg1*$^{Cre/+}$;*Fgfr1*$^{flox/+}$, and

1170 *Foxg1*$^{Cre/+}$;*Fgfr1*$^{flox/-}$ cochleae results were analyzed by one-way ANOVA. P values

1171 shown are from the t test and ANOVA. * indicates $p < 0.05$ from Student's t test or

1172 Tukey's HSD (ANOVA post-hoc); n.s., not significant. Error bars, mean ± SD.

1173 (G) Schematic showing the positions of basal, middle, and apical turns along the cochlear

1174 duct.

1175 See also S1 Fig.

1176

1177 **Fig 2. FGFR1 but not FGF20 regulates *Sox2* expression**

1178 (A) Sections through the middle turn of E14.5 cochlear ducts from *Fgf20*$^{+/-}$, *Fgf20*$^{-/-}$,

1179 *Foxg1*$^{Cre/+}$;*Fgfr1*$^{flox/+}$, and *Foxg1*$^{Cre/+}$;*Fgfr1*$^{flox/-}$ mice. RNA in situ hybridization (top) and

1180 immunofluorescence for *Sox2* (red, bottom), which is expressed in the prosensory

1181 domain at this stage. Refer to schematic in (C).

1182 (B) Immunofluorescence for CDKN1B (green) in sections through the basal, middle, and
1183 apical turns of E14.5 *Fgf20*$^{+/-}$, *Fgf20*$^{-/-}$, *Foxg1*$^{Cre/+}$;*Fgfr1*$^{flox/+}$, and *Foxg1*$^{Cre/+}$;*Fgfr1*$^{flox/-}$
1184 cochleae.
1185 (C) Schematic of a cross section through the middle turn of the E14.5 cochlear duct,
1186 showing the location of the prosensory domain (PD). Neural indicates the side of the
1187 duct towards the spiral ganglion cells; abneural indicates away.
1188 (D) A model of genetic pathways during organ of Corti development. Ligand X/FGFR1
1189 signaling regulates *Sox2* expression during prosensory specification; FGF20/FGFR1
1190 signaling regulates differentiation. Ligand X may include FGF20, along with another
1191 functionally redundant ligand.
1192 DAPI, nuclei (blue). Scale bar, 100 μm. See also S2 Fig.
1193

1194 **Fig 3. Genetic rescue of the Fgf20-KO phenotype suggests that FGF20 is required**
1195 **for differentiation**

1196 (A, B) Whole mount cochlea from P0 *Fgf20*$^{+/-}$;*ROSA*^{rtTA} (Fgf20-het), *Fgf20*$^{+/-}$;*ROSA*^{rtTA}; TRE-
1197 Fgf9-IRES-eGfp (Fgf9-OA), *Fgf20*$^{-/-}$;*ROSA*^{rtTA} (Fgf20-null), and *Fgf20*$^{-/-}$;*ROSA*^{rtTA}; TRE-
1198 Fgf9-IRES-eGfp (Fgf20-rescue) mice showing (A) inner and outer hair cells (phalloidin,
1199 green) separated by inner pillar cells (p75NTR, red) and (B) supporting cells (Prox1 and
1200 Sox2, green/yellow). Images from basal, middle, and apical turns of the cochlea are
1201 shown. Fgf20-rescue cochleae from four different doxycycline chow (Dox) regimens are
1202 shown (E13.5-E15.5, E13.5, E14.5, and E15.5). Fgf20-het, Fgf9-OA, and Fgf20-null
1203 cochleae shown are from the E13.5-E15.5 Dox regimen. Scale bar, 100 μm.
1204 (C) Quantification of outer hair cells (OHC) and supporting cells (SC) from P0 Fgf9-OA (Dox
1205 regimen: E13.5-E15.5), Fgf20-null (Dox regimen: E13.5-E15.5), and Fgf20-rescue (all
1206 four Dox regimens) cochleae, presented as a percentage of the number of cells in

1207 Fgf20-het cochleae from the same Dox regimen. * indicates $p < 0.05$ compared to Fgf20-
1208 null cochleae from the same Dox regimen; ^ indicates $p < 0.05$ compared to Fgf20-het
1209 cochleae from the same Dox regimen; Tukey's HSD (one-way ANOVA post-hoc).
1210 See also S3 Fig.
1211

1212 **Fig 4. Decrease in Sox2 expression results in similar phenotypes as disruptions**
1213 **to FGFR1 signaling**

1214 (A, B) Whole mount cochlea from P0 mice from the *Sox2* allelic series (in order of highest to
1215 lowest levels of *Sox2* expression: $Sox2^{+/+}$, $Sox2^{Ysb/+}$, $Sox2^{Ysb/Ysb}$, and $Sox2^{Ysb/-}$) showing
1216 (A) inner and outer hair cells (phalloidin, green) separated by inner pillar cells (p75NTR,
1217 red) and (B) supporting cells (Prox1 and Sox2, green/yellow). Magnifications show the
1218 basal, middle, and apical turns of the cochlea. Arrowheads indicate ectopic inner hair
1219 cells. Scale bar, 100 μm (magnifications), 1 mm (whole).
1220 (C-F) Quantification of (C) cochlear duct length, (D) total inner hair cells (IHCs) and IHCs per
1221 100 μm of the cochlear duct, (E) total outer hair cells (OHCs) and OHCs per 100 μm,
1222 and (F) total supporting cells (SCs) and SCs per 100 μm at P0. P values shown are from
1223 one-way ANOVA. * indicates $p < 0.05$ from Tukey's HSD (ANOVA post-hoc). Error bars,
1224 mean ± SD.
1225 See also S4 Fig.
1226

1227 **Fig 5. Decrease in levels of Sox2 expression delays prosensory specification**

1228 (A) Serial sections (1-6) through the duct of E14.5 and E15.5 $Sox2^{Ysb/+}$ and $Sox2^{Ysb/-}$
1229 cochleae. Immunofluorescence for Ki67 (red) and DAPI (nuclei, cyan). Cochlear
1230 epithelium is outlined. Bracket indicates prosensory domain. * indicates shift of
1231 prosensory nuclei away from the luminal surface of the epithelium. N, neural side. Scale

1232 bar, 100 μm. Whole mount cochlear duct schematics show relative positions of the serial
1233 sections and progression of cell cycle exit (green arrow).
1234 (B) A model of organ of Corti development showing embryonic staging (x-axis) and location
1235 along the cochlear duct (basal, middle, and apical turns, y-axis). Development occurs in
1236 two stages: unspecified progenitors (tan shading) undergo specification and cell cycle
1237 exit to become prosensory cells (green shading), which then differentiate into hair cells
1238 and supporting cells (HCs & SCs; red shading). In wildtype cochleae, cell cycle exit
1239 (indicating completion of specification) begins at the apex of the cochlea and proceeds
1240 basally. Afterwards, differentiation initiates at the mid-base of the cochlea and proceeds
1241 basally and apically. Temporal buffer (green shading) refers to the time between cell
1242 cycle exit and initiation of differentiation. In *Sox2* hypomorph cochleae, specification and
1243 cell cycle exit are delayed, resulting in failure to complete specification before initiation of
1244 differentiation towards the basal end of the cochlea (crosshatch pattern).
1245 See also S5 Fig.
1246

1247 **Fig 6. *Sox2* is upstream of *Fgf20***

1248 (A-C) Sections through the middle turn of E14.5 cochleae.
1249 (A) RNA in situ hybridization for *Etv4* and *Etv5* in *Sox2*$^{Ysb/+}$ and *Sox2*$^{Ysb/-}$ cochleae. The two
1250 brackets indicate *Etv4/5* expression in the outer sulcus (OS, left) and prosensory domain
1251 (PD, right). Refer to schematic at the bottom right of the figure.
1252 (B) RNA in situ hybridization for *Fgfr1* and *Fgf20* in *Sox2*$^{Ysb/+}$ and *Sox2*$^{Ysb/-}$ cochleae. Bracket
1253 indicates *Fgfr1*/*Fgf20* expression in the prosensory domain.
1254 (C) RNA in situ hybridization for *Fgf20* in *Foxg1*$^{Cre/+}$;*Fgfr1*$^{flox/+}$ and *Foxg1*$^{Cre/+}$;*Fgfr1*$^{flox/-}$
1255 cochleae. Bracket indicates *Fgf20* expression in the prosensory domain.
1256 (D) Serial sections (1-6) through the duct of E14.5 *Fgf20*$^{+/-}$ and *Fgf20*$^{-/-}$ cochleae.
1257 Immunofluorescence for Ki67 (red) and DAPI (nuclei, cyan). Cochlear epithelium is

1258 outlined. Bracket indicates prosensory domain. * indicates shift of prosensory nuclei
1259 away from the luminal surface of the epithelium. N, neural side. Scale bar, 100 μm.
1260 Whole mount cochlear duct schematics show relative positions of the serial sections and
1261 progression of cell cycle exit (green arrow).
1262 OS, outer sulcus; PD, prosensory domain; KO, Kölliker's organ. Scale bar, 100 μm. See also S6
1263 Fig.
1264

1265 **Fig 7. *Sox2* and *Fgf20* interact during cochlea development**

1266 (A, B) Whole mount cochlea from P0 *Fgf20*$^{+/-}$;*Sox2*$^{Ysb/+}$, *Fgf20*$^{+/-}$;*Sox2*$^{Ysb/Ysb}$, *Fgf20*$^{-/-}$;*Sox2*$^{Ysb/+}$,
1267 and *Fgf20*$^{-/-}$;*Sox2*$^{Ysb/Ysb}$ mice showing (A) inner and outer hair cells (phalloidin, green)
1268 separated by inner pillar cells (p75NTR, red) and (B) supporting cells (Prox1 and Sox2,
1269 green/yellow). Magnifications show the basal, middle, and apical turns of the cochlea.
1270 Arrowheads indicate ectopic inner hair cells. Scale bar, 100 μm (magnifications), 1 mm
1271 (whole).
1272

1273 **Fig 8. *Sox2* and *Fgf20* interact during cochlea development—quantitative analysis**

1274 (A) P values from two-way ANOVA analyzing the quantification results in (B-E). The two
1275 factors analyzed are *Fgf20* (*Fgf20*$^{+/+}$, *Fgf20*$^{+/-}$, *Fgf20*$^{-/-}$) and *Sox2* (*Sox2*$^{+/+}$, *Sox2*$^{Ysb/+}$,
1276 *Sox2*$^{Ysb/Ysb}$) gene dosage. A p value < 0.05 (yellow highlight) for *Fgf20* or *Sox2* indicates
1277 that the particular factor (independent variable) has a statistically significant effect on the
1278 measurement (dependent variable). Whereas a p value < 0.05 (orange highlight) for
1279 Interaction indicates a statistically significant interaction between the effects of the two
1280 factors on the measurement.
1281 (B-E) Quantification of (B) cochlear duct length, (C) total inner hair cells (IHCs) and IHCs per
1282 100 μm of the cochlear duct, (D) total outer hair cells (OHCs) and OHCs per 100 μm,

1283 and (E) total supporting cells (SCs) and SCs per 100 μm at P0 in *Fgf20*$^{+/+}$;*Sox2*$^{+/+}$,
1284 *Fgf20*$^{+/+}$;*Sox2*$^{Ysb/+}$, *Fgf20*$^{+/-}$;*Sox2*$^{+/+}$, *Fgf20*$^{+/-}$;*Sox2*$^{Ysb/+}$, *Fgf20*$^{+/+}$;*Sox2*$^{Ysb/Ysb}$,
1285 *Fgf20*$^{+/-}$;*Sox2*$^{Ysb/Ysb}$, *Fgf20*$^{-/-}$;*Sox2*$^{+/+}$, *Fgf20*$^{-/-}$;*Sox2*$^{Ysb/+}$, and *Fgf20*$^{-/-}$;*Sox2*$^{Ysb/Ysb}$ cochleae.
1286 Error bars, mean ± SD.

1287 (F) Results from post-hoc Tukey's HSD analyzing the quantification results in (B-E). Letters
1288 (L, I, J, O, P, S, T; representing each measurement in panels B-E) indicate a statistically
1289 significant decrease ($p < 0.05$) when comparing the row genotype against the column
1290 genotype. L, cochlear length; I, total IHCs; J, IHCs/100 μm; O, total OHCs; P, OHCs/100
1291 μm; S, total SCs; T, SCs/100 μm.

1292 See also S7 and S8 Figs.

1293

1294 **Fig 9. Loss of Fgf20 does not further delay prosensory specification in Sox2**
1295 **hypomorph cochleae**

1296 (A) The *Fgf20*$^{-/-}$, *Foxg1*$^{Cre/+}$;*Fgfr1*$^{flox/-}$, *Fgf20*$^{-/-}$;*Sox2*$^{Ysb/Ysb}$, and *Sox2*$^{Ysb/-}$ cochleae phenotypes
1297 lie along a continuum, preferentially affecting outer and basal cochlear sensory
1298 epithelium, likely attributable to varying *Sox2* levels on an *Fgf20*-null background.

1299 (B) Serial sections (1-6) through the duct of E14.5 *Fgf20*$^{+/-}$;*Sox2*$^{Ysb/+}$, *Fgf20*$^{+/-}$;*Sox2*$^{Ysb/Ysb}$,
1300 *Fgf20*$^{-/-}$;*Sox2*$^{Ysb/+}$, and *Fgf20*$^{-/-}$;*Sox2*$^{Ysb/Ysb}$ cochleae. Immunofluorescence for Ki67 (red)
1301 and DAPI (nuclei, cyan). Cochlear epithelium is outlined. Bracket indicates prosensory
1302 domain. * indicates shift of prosensory nuclei away from the luminal surface of the
1303 epithelium. N, neural side. Whole mount cochlear duct schematics show relative
1304 positions of the serial sections and progression of cell cycle exit (green arrow). Note:
1305 unlike in Fig 7, we have switched the placement of images from *Fgf20*$^{-/-}$;*Sox2*$^{Ysb/+}$ and
1306 *Fgf20*$^{+/-}$;*Sox2*$^{Ysb/Ysb}$ cochleae to facilitate comparison.

1307 Scale bar, 100 μm. See also S10 Fig.

1308

1309 **Fig 10. Fgf20-KO organ of Corti exhibits premature differentiation**

1310 (A) RNA in situ hybridization for *Hey1* and *Hey2* on sections through the middle turn of

1311 E14.5 *Fgf20*$^{+/-}$ and *Fgf20*$^{-/-}$ cochleae.

1312 (B, C) Immunofluorescence for Myo6 (red) on "mid-modiolar" sections through the (B) E14.5

1313 *Fgf20*$^{+/-}$ and *Fgf20*$^{-/-}$ cochleae, and (C) E15.0 Fgf20-het (*Fgf20*$^{Cre/+}$;*ROSA*$^{rtTA/+}$), Fgf20-null

1314 (*Fgf20*$^{Cre/\beta gal}$;*ROSA*$^{rtTA/+}$), Fgf9-OA (*Fgf20*$^{Cre/+}$;*ROSA*$^{rtTA/+}$;TRE-Fgf9-IRES-eGfp), Fgf20-

1315 rescue (*Fgf20*$^{Cre/\beta gal}$;*ROSA*$^{rtTA/+}$;TRE-Fgf9-IRES-eGfp) cochleae (Dox from E13.5 to

1316 E15.0), with magnification. The number of cochleae containing Myo6-expressing cells

1317 out of the total number of cochleae examined for each genotype are shown below each

1318 panel. Arrows indicate Myo6-expressing hair cells. DAPI, nuclei (blue).

1319 OS, outer sulcus; PD, prosensory domain; KO, Kölliker's organ. Scale bar, 100 μm.

1320

1321 **Fig 11. *Sox2* and *Fgf20* interact to modulate a temporal buffer between**

1322 **specification and differentiation**

1323 Model of the roles of *Sox2* and *Fgf20* in organ of Corti development, which occurs in two stages:

1324 unspecified progenitors (tan shading) undergo specification and cell cycle exit to become

1325 prosensory cells (green shading), which then differentiate into hair cells and supporting cells

1326 (HCs & SCs; red shading). In wildtype cochleae, cell cycle exit (indicating completion of

1327 specification) begins at the apex of the cochlea and proceeds basally. Afterwards, differentiation

1328 initiates at the mid-base of the cochlea and proceeds basally and apically. The prosensory cells

1329 exist within a temporal buffer (green shading), defined as the time between cell cycle exit and

1330 initiation of differentiation. In *Sox2*/*Fgf20* mutant cochleae, decrease in levels of *Sox2*

1331 expression in the developing cochlea leads to delayed prosensory specification and cell cycle

1332 exit (arrow 1), while loss of *Fgf20* leads to premature onset of differentiation at the basal and

1333 mid-basal cochlear turns (arrow 2) as well as delayed differentiation at the apical turn (arrow 3).
1334 Loss of both *Sox2* and *Fgf20* leads to loss of the temporal buffer between specification and
1335 differentiation towards the base of the cochlear duct, disrupting the development of HCs and
1336 SCs in the basal region (crosshatch pattern).
1337
1338

1339 Supplemental figure titles and legends

1340

1341 **S1 Fig.**

1342 (A-C) Quantification of length-normalized number of (A) inner hair cells (IHCs/100 μm), (B)
1343 outer hair cells (OHCs/100 μm), and (C) supporting cells (SCs/100 μm) in the basal,
1344 middle, and apical turns of P0 cochleae from *Fgf20*$^{+/-}$, *Fgf20*$^{-/-}$ *Fgfr1*$^{flox/+}$, *Fgfr1*$^{flox/-}$,
1345 *Foxg1*$^{Cre/+}$;*Fgfr1*$^{flox/+}$, and *Foxg1*$^{Cre/+}$;*Fgfr1*$^{flox/-}$ mice. *Fgf20*$^{+/-}$ and *Fgf20*$^{-/-}$ cochleae were
1346 analyzed by unpaired Student's t test; *Fgfr1*$^{flox/+}$, *Fgfr1*$^{flox/-}$, *Foxg1*$^{Cre/+}$;*Fgfr1*$^{flox/+}$, and
1347 *Foxg1*$^{Cre/+}$;*Fgfr1*$^{flox/-}$ cochleae were analyzed by one-way ANOVA. P values shown are
1348 from the t test and ANOVA. * indicates $p < 0.05$ from Student's t test or Tukey's HSD
1349 (ANOVA post-hoc); n.s., not significant. Error bars, mean ± SD.
1350 (D) Schematic showing the positions of basal, middle, and apical turns along the cochlear
1351 duct. Apical tip refers to the apical end of the cochlea.
1352 (E) Whole mount cochlea from P0 *Fgf20*$^{+/-}$, *Fgf20*$^{-/-}$, *Foxg1*$^{Cre/+}$;*Fgfr1*$^{flox/+}$, and
1353 *Foxg1*$^{Cre/+}$;*Fgfr1*$^{flox/-}$ mice showing immunofluorescence for phalloidin (green) and
1354 p75NTR (red) at the apical tip of the cochlea. T, towards the tip. Scale bar, 100 μm.
1355

1356 **S2 Fig.**

1357 (A, B) Sections through the middle turn of E14.5 cochlear ducts from *Fgf20*$^{+/-}$, *Fgf20*$^{-/-}$,

1358 *Foxg1*$^{Cre/+}$;*Fgfr1*$^{flox/+}$, and *Foxg1*$^{Cre/+}$;*Fgfr1*$^{flox/-}$ mice. Scale bar, 100 μm. Refer to

1359 schematic below. OS, outer sulcus; PD, prosensory domain; KO, Kölliker's organ.

1360 (A) RNA in situ hybridization for *Etv4* and *Etv5.* The two brackets indicate *Etv4/5* expression

1361 in the outer sulcus (OS, left) and prosensory domain (PD, right; lost in *Fgf20*$^{-/-}$ and

1362 *Foxg1*$^{Cre/+}$;*Fgfr1*$^{flox/-}$ cochleae).

1363 (B) EdU-incorporation (green). Dashed region indicates Kölliker's organ (KO). DAPI, nuclei

1364 (blue).

1365

1366 **S3 Fig.**

1367 Quantification of length-normalized number of inner hair cells (IHCs/100 μm), outer hair cells

1368 (OHCs/100 μm), and supporting cells (SCs/100 μm) overall (along the entire cochlea; top three

1369 graphs) and in the basal, middle, and apical turns (bottom three graphs) of P0 cochleae from

1370 *Fgf20*$^{+/-}$;*ROSA*^{rtTA} (Fgf20-het), *Fgf20*$^{+/-}$;*ROSA*^{rtTA}; TRE-Fgf9-IRES-eGfp (Fgf9-OA), *Fgf20*$^{-}$

1371 $^{/-}$;*ROSA*^{rtTA} (Fgf20-null), and *Fgf20*$^{-/-}$;*ROSA*^{rtTA}; TRE-Fgf9-IRES-eGfp (Fgf20-rescue) mice. Dox

1372 regimens: E13.5-E15.5, E13.5, E14.5, or E15.5. P values shown are from one-way ANOVA. *

1373 indicates $p < 0.05$ from Tukey's HSD (ANOVA post-hoc); n.s., not significant. Error bars, mean ±

1374 SD. Summarized in Fig 3C.

1375

1376 **S4 Fig.**

1377 (A-C) Quantification of length-normalized number of (A) inner hair cells (IHCs/100 μm), (B)

1378 outer hair cells (OHCs/100 μm), and (C) supporting cells (SCs/100 μm) in the basal,

1379 middle, and apical turns of P0 cochleae from *Sox2*$^{+/+}$, *Sox2*$^{Ysb/+}$, *Sox2*$^{Ysb/Ysb}$, and *Sox2*$^{Ysb/-}$

1380 mice. P values shown are from one-way ANOVA. * indicates $p < 0.05$ from Tukey's HSD
1381 (ANOVA post-hoc); n.s., not significant. Error bars, mean ± SD.
1382 (D) Whole mount cochlea from P0 *Sox2*$^{Ysb/-}$ mice showing presence of inner and outer hair
1383 cells (phalloidin/p75NTR) and supporting cells (Prox1/Sox2, in a different cochlea) at the
1384 basal tip. Schematic shows the location of sensory epithelium at the apical turn and
1385 basal tip of *Sox2*$^{Ysb/-}$ cochleae. Scale bar, 1 mm (whole), 100 μm (basal tip).
1386
1387 **S5 Fig.**
1388 (A, B) Immunofluorescence for (A) Sox2 (red) and (B) CKDN1B (green) in sections through the
1389 basal, middle, and apical turns of E14.5 *Sox2*$^{Ysb/+}$ and *Sox2*$^{Ysb/-}$ cochleae.
1390 (C) Immunofluorescence for Ki67 (red) on serial "mid-modiolar" sections through the E14.5
1391 and E15.5 *Sox2*$^{Ysb/+}$ and *Sox2*$^{Ysb/-}$ cochleae. Brackets indicate prosensory domain. Nine
1392 sections through the length of the cochlear duct are labeled. See whole mount cochlear
1393 duct schematic (lower left) for relative positions of the sections.
1394 DAPI, nuclei (blue). Scale bar, 100 μm.
1395
1396 **S6 Fig.**
1397 (A) Immunofluorescence for Ki67 (red) on serial "mid-modiolar" sections through the E14.5
1398 *Fgf20*$^{+/-}$ and *Fgf20*$^{-/-}$ cochleae. Brackets indicate prosensory domain. Nine sections
1399 through the length of the cochlear duct are labeled. See whole mount cochlear duct
1400 schematic (right) for relative positions of the sections.
1401 (B) EdU-incorporation (green) in sections through the middle turn of E14.5 *Sox2*$^{Ysb/+}$ and
1402 *Sox2*$^{Ysb/-}$ cochleae. Dashed region indicates Kölliker's organ (KO). Bracket indicates part
1403 of Kölliker's organ without EdU-incorporating cells in *Sox2*$^{Ysb/-}$ cochleae.

1404 OS, outer sulcus; PD, prosensory domain; KO, Kölliker's organ. DAPI, nuclei (blue). Scale bar,
1405 100 μm.
1406
1407 **S7 Fig.**
1408 (A) P values from two-way ANOVA analyzing the quantification in (B-D). The two factors
1409 analyzed are *Fgf20* (*Fgf20*$^{+/+}$, *Fgf20*$^{+/-}$, *Fgf20*$^{-/-}$) and *Sox2* (*Sox2*$^{+/+}$, *Sox2*$^{Ysb/+}$, *Sox2*$^{Ysb/Ysb}$)
1410 gene dosage. A p value < 0.05 (yellow highlight) for *Fgf20* or *Sox2* indicates that the
1411 particular factor (independent variable) has a statistically significant effect on the
1412 measurement (dependent variable). Whereas a p value < 0.05 for Interaction indicates a
1413 statistically significant interaction between the effects of the two factors on the
1414 measurement.
1415 (B-D) Quantification of length-normalized number of (B) inner hair cells (IHCs/100 μm), (C)
1416 outer hair cells (OHCs/100 μm), and (D) supporting cells (SCs/100 μm) in the basal,
1417 middle, and apical turns of P0 cochleae from *Fgf20*$^{+/+}$;*Sox2*$^{+/+}$, *Fgf20*$^{+/+}$;*Sox2*$^{Ysb/+}$,
1418 *Fgf20*$^{+/-}$;*Sox2*$^{+/+}$, *Fgf20*$^{+/-}$;*Sox2*$^{Ysb/+}$, *Fgf20*$^{+/+}$;*Sox2*$^{Ysb/Ysb}$, *Fgf20*$^{+/-}$;*Sox2*$^{Ysb/Ysb}$, *Fgf20*$^{-/-}$;*Sox2*$^{+/+}$, *Fgf20*$^{-/-}$;*Sox2*$^{Ysb/+}$, and *Fgf20*$^{-/-}$;*Sox2*$^{Ysb/Ysb}$ mice. Error bars, mean ± SD.
1419
1420
1421 **S8 Fig.**
1422 Results from post-hoc Tukey's HSD analyzing the quantification results in (B-D). Letters (L, I, J,
1423 O, P, S, T; representing each measurement in S7B-S7D Figs) indicate a statistically significant
1424 decrease (p < 0.05) when comparing the row genotype against the column genotype. L,
1425 cochlear length; I, IHCs/100 μm; O, OHCs/100 μm; S, SCs/100 μm.
1426

1427 **S9 Fig.**

1428 (A) Whole mount cochlea from P0 *Fgf20*$^{+/+}$;*Sox2*$^{+/+}$, *Fgf20*$^{+/-}$;*Sox2*$^{+/+}$, *Fgf20*$^{+/+}$;*Sox2*$^{Ysb/+}$, and
1429 *Fgf20*$^{+/-}$;*Sox2*$^{Ysb/+}$ mice showing inner and outer hair cells (phalloidin, green) separated
1430 by inner pillar cells (p75NTR, red). Magnifications show the basal, middle, and apical
1431 turns of the cochlea. Scale bar, 100 μm (magnifications), 1 mm (whole); arrowheads
1432 indicate ectopic inner hair cells.

1433 (B-F) Quantification of (B) cochlear duct length, (C) total inner hair cells (IHCs) and IHCs per
1434 100 μm of the cochlear duct, (D) total outer hair cells (OHCs) and OHCs per 100 μm,
1435 and (E) IHCs/100 μm and (F) OHCs/100 μm in the basal, middle, and apical turns at P0.
1436 P values shown are from one-way ANOVA. * indicates $p < 0.05$ from Tukey's HSD
1437 (ANOVA post-hoc); n.s., not significant. Error bars, mean ± SD.

1438

1439 **S10 Fig.**

1440 (A, B) Immunofluorescence for (A) Sox2 (red) and (B) CDKN1B (green) in sections through the
1441 basal, middle, and apical turns of E14.5 *Fgf20*$^{+/-}$;*Sox2*$^{Ysb/+}$, *Fgf20*$^{-/-}$;*Sox2*$^{Ysb/+}$,
1442 *Fgf20*$^{+/-}$;*Sox2*$^{Ysb/Ysb}$, and *Fgf20*$^{-/-}$;*Sox2*$^{Ysb/Ysb}$ cochleae.

1443 (C) EdU-incorporation (green) in sections through the middle turn of E14.5 *Fgf20*$^{+/-}$;*Sox2*$^{Ysb/+}$,
1444 *Fgf20*$^{-/-}$;*Sox2*$^{Ysb/+}$, *Fgf20*$^{+/-}$;*Sox2*$^{Ysb/Ysb}$, and *Fgf20*$^{-/-}$;*Sox2*$^{Ysb/Ysb}$ cochleae. Dashed region
1445 indicates Kölliker's organ (KO).

1446 (D) Immunofluorescence for Ki67 (red) on serial "mid-modiolar" sections through the E14.5
1447 *Fgf20*$^{+/-}$;*Sox2*$^{Ysb/+}$, *Fgf20*$^{-/-}$;*Sox2*$^{Ysb/+}$, *Fgf20*$^{+/-}$;*Sox2*$^{Ysb/Ysb}$, and *Fgf20*$^{-/-}$;*Sox2*$^{Ysb/Ysb}$
1448 cochleae. Brackets indicate prosensory domain. Nine sections through the length of the
1449 cochlear duct are labeled. See whole mount cochlear duct schematic (upper right) for
1450 relative positions of the sections.

1451 Note: unlike in Fig 7, we have switched the placement of images from *Fgf20*$^{-/-}$;*Sox2*$^{Ysb/+}$ and

1452 *Fgf20*$^{+/-}$;*Sox2*$^{Ysb/Ysb}$ cochleae to facilitate comparison. OS, outer sulcus; PD, prosensory domain;

1453 KO, Kölliker's organ. DAPI, nuclei (blue). Scale bar, 100 μm.

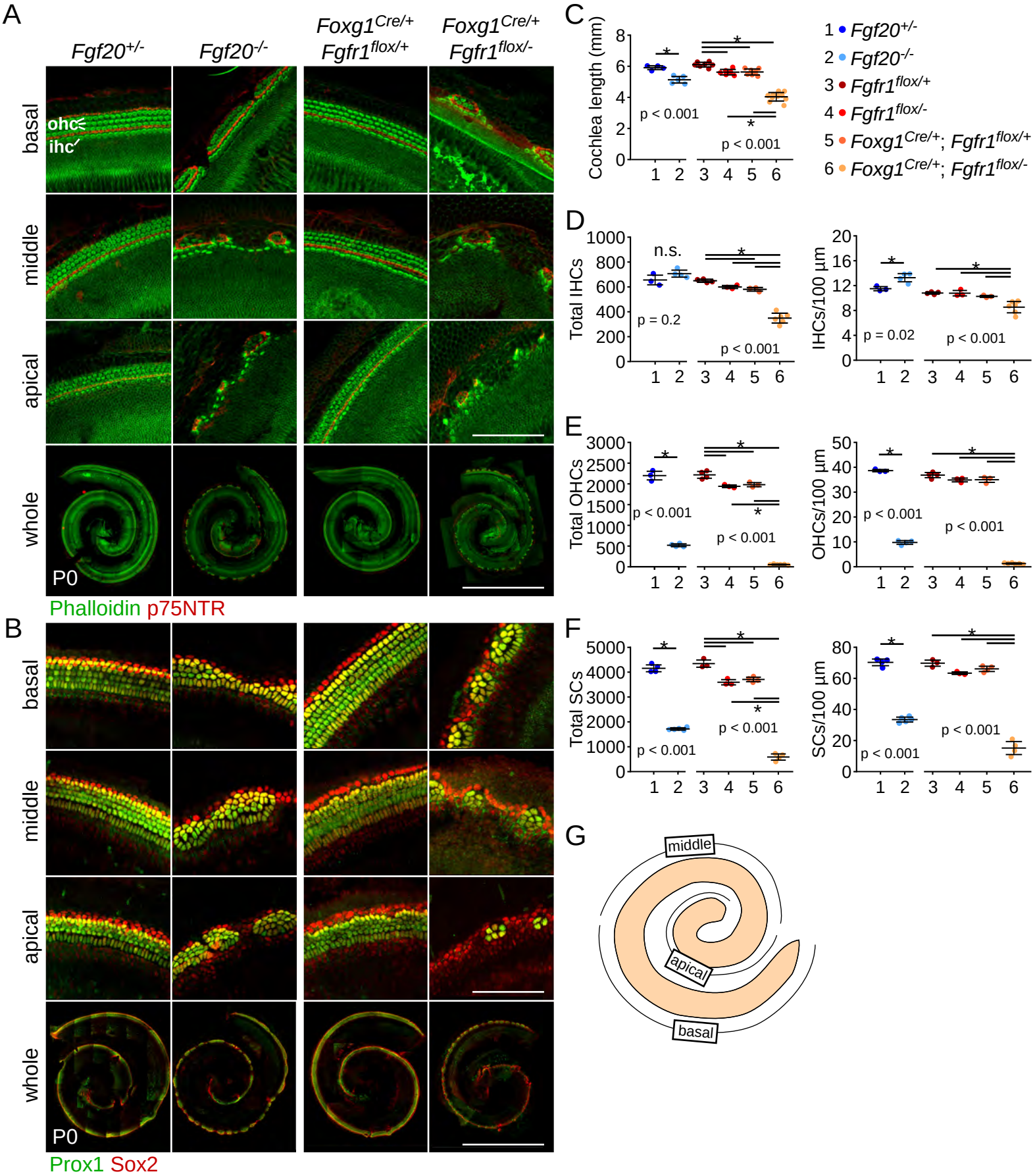
A
Fgf20+/-
Fgf20-/-
Foxg1Cre/+ Fgfr1flox/+
Foxg1Cre/+ Fgfr1flox/-
basal
middle
apical
whole
ohc
ihc
P0
Phalloidin p75NTR
B
basal
middle
apical
whole
P0
Prox1 Sox2
C
Cochlea length (mm)
p < 0.001
p < 0.001
1 Fgf20+/-
2 Fgf20-/-
3 Fgfr1flox/+
4 Fgfr1flox/-
5 Foxg1Cre/+; Fgfr1flox/+
6 Foxg1Cre/+; Fgfr1flox/-
D
Total IHCs
n.s.
p = 0.2
p < 0.001
IHCs/100 µm
p = 0.02
p < 0.001
E
Total OHCs
p < 0.001
p < 0.001
OHCs/100 µm
p < 0.001
p < 0.001
F
Total SCs
p < 0.001
p < 0.001
SCs/100 µm
p < 0.001
p < 0.001
G
middle
apical
basal

Fig 2

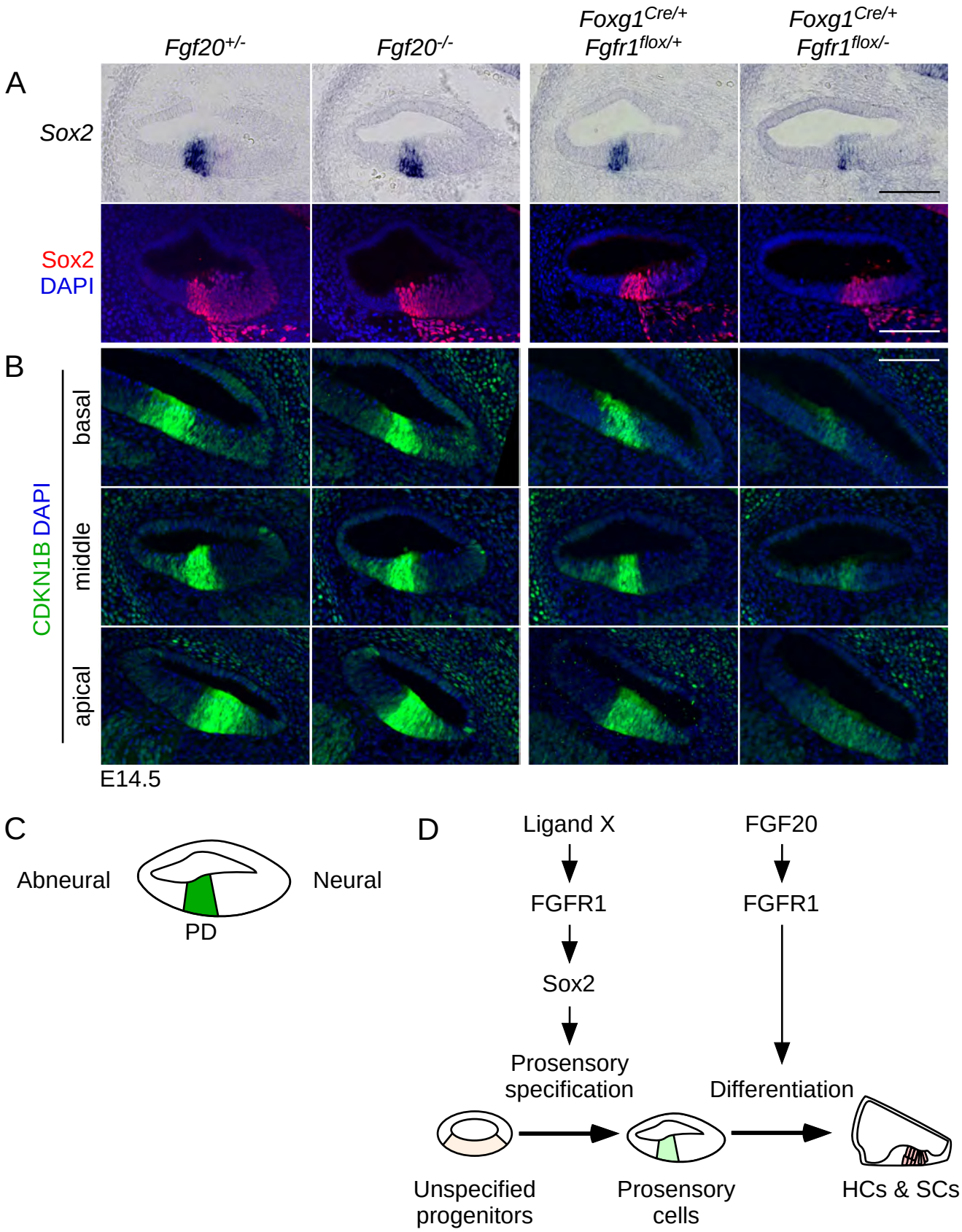
Fgf20+/-
Fgf20-/-
Foxg1Cre/+ Fgfr1flox/+
Foxg1Cre/+ Fgfr1flox/-
A
Sox2
Sox2
DAPI
B
CDKN1B DAPI
basal
middle
apical
E14.5
C
Abneural
Neural
PD
D
Ligand X
FGF20
FGFR1
FGFR1
Sox2
Prosensory specification
Differentiation
Unspecified progenitors
Prosensory cells
HCs & SCs

Fig 3

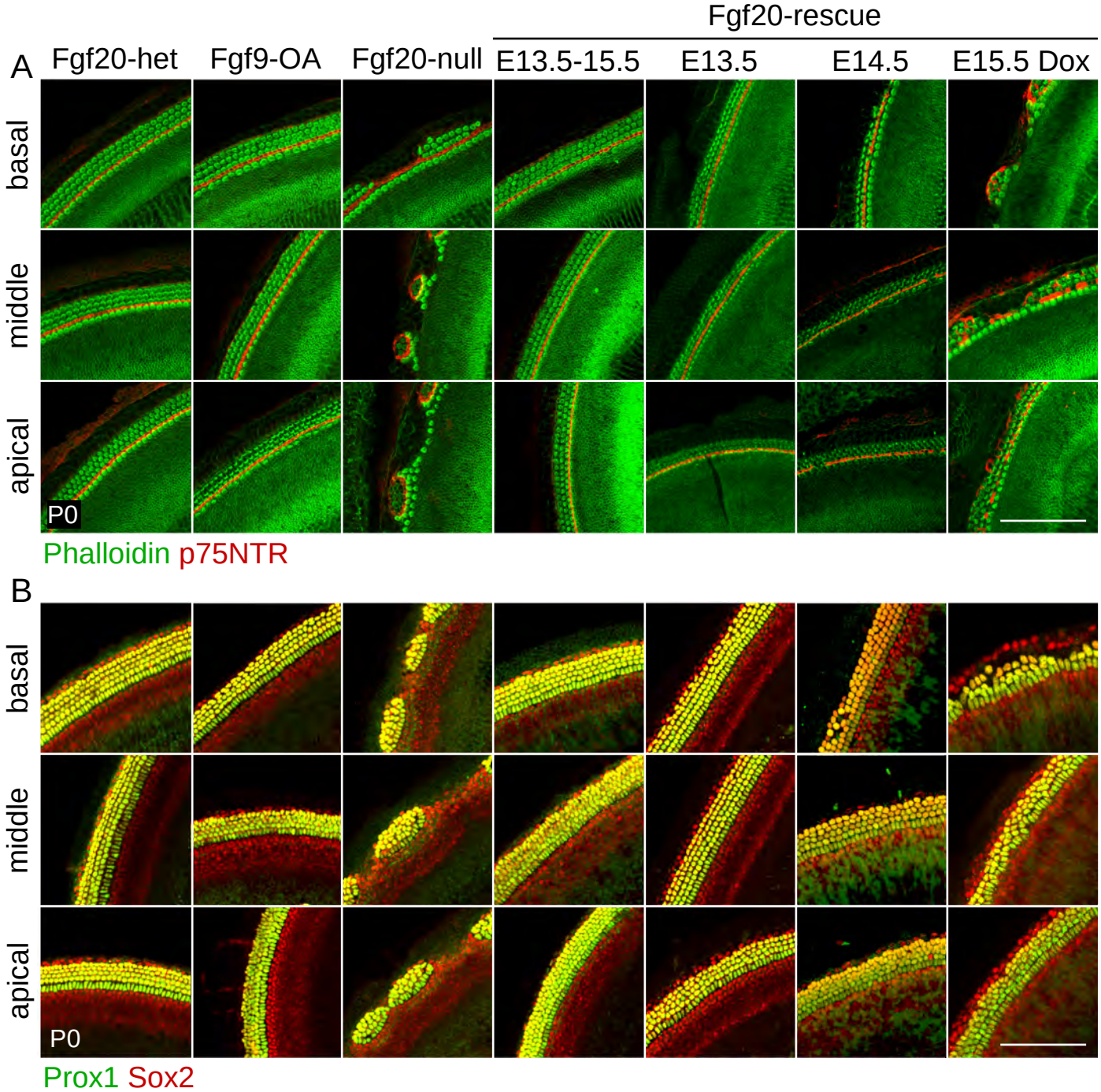

C

		Fgf9-OA	Fgf20-null	Fgf20-rescue E13.5-15.5	Fgf20-rescue E13.5	Fgf20-rescue E14.5	Fgf20-rescue E15.5 Dox
OHC	basal	95.3%*	48.6%^	105.8%*	102.4%*	76.2%*	41.7%^
	middle	99.6%*	32.4%^	108.2%*	89.0%*	94.4%*	44.7%^
	apical	97.1%*	29.0%^	101.3%*	81.2%*^	94.8%*	75.7%*^
SC	basal	99.0%*	44.1%^	103.4%*	85.6%*^	66.9%^	47.1%^
	middle	97.6%*	40.3%^	102.8%*	88.7%*	80.7%*	49.5%^
	apical	88.0%*	28.4%^	94.0%*	83.3%	74.7%	70.9%*^

<60.0%	60.0-69.9%	70.0-79.9%	80.0-89.9%	>90.0%

Fig 4

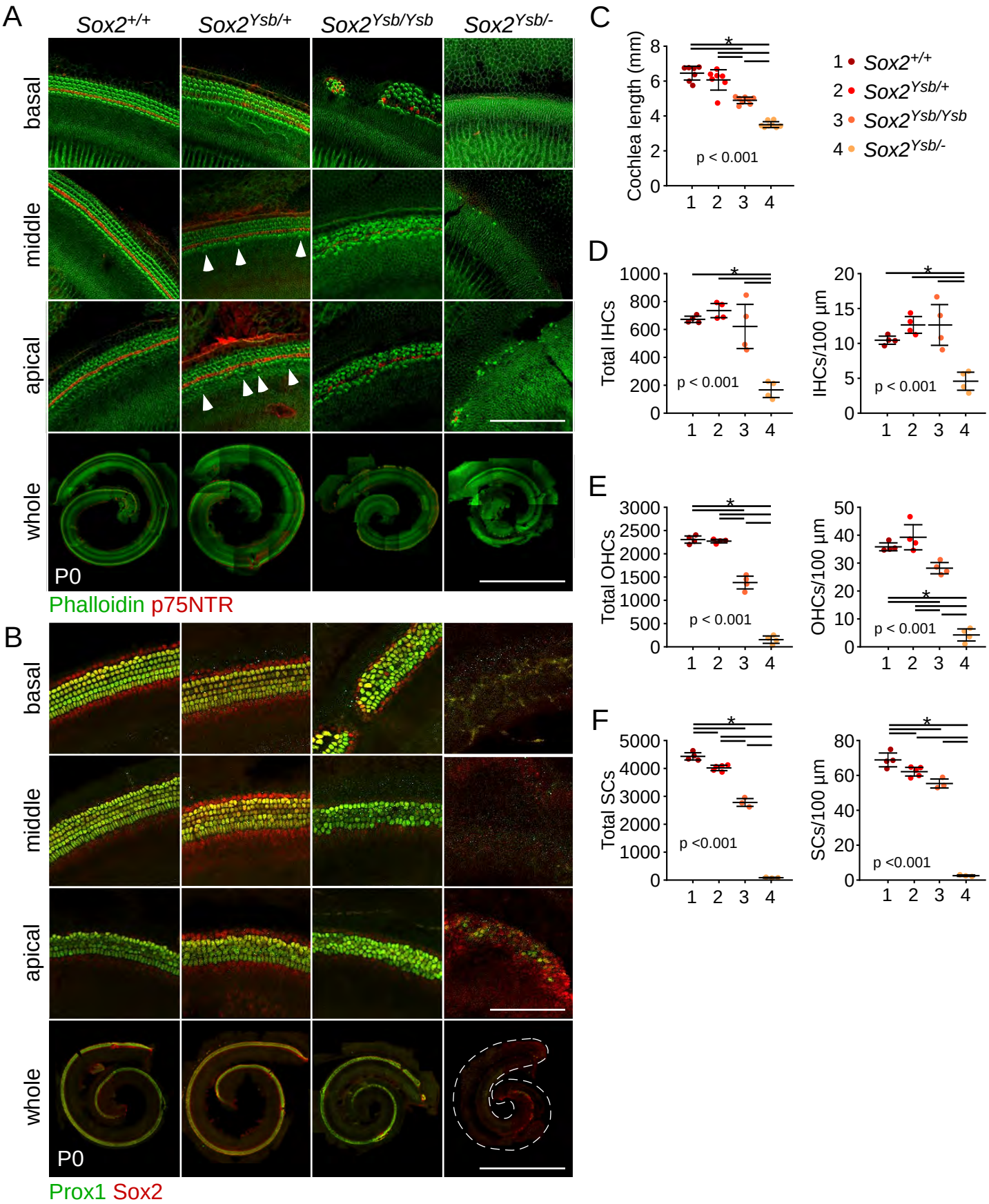
A
Sox2+/+
Sox2Ysb/+
Sox2Ysb/Ysb
Sox2Ysb/-
basal
middle
apical
whole
P0
Phalloidin p75NTR
B
basal
middle
apical
whole
P0
Prox1 Sox2
C
Cochlea length (mm)
p < 0.001
1 Sox2+/+
2 Sox2Ysb/+
3 Sox2Ysb/Ysb
4 Sox2Ysb/-
D
Total IHCs
p < 0.001
IHCs/100 µm
p < 0.001
E
Total OHCs
p < 0.001
OHCs/100 µm
p < 0.001
F
Total SCs
p <0.001
SCs/100 µm
p <0.001

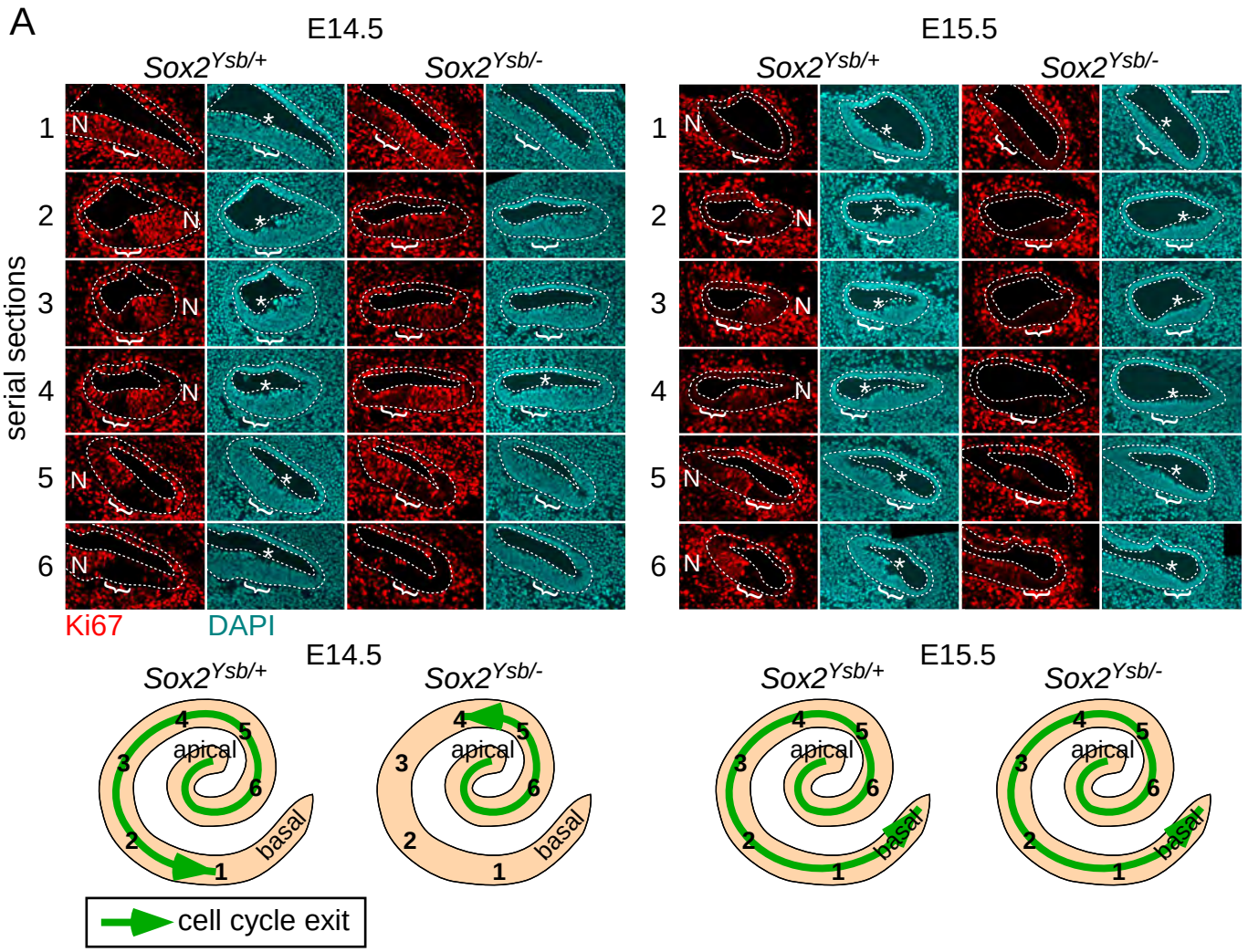
A
E14.5
E15.5
Sox2Ysb/+
Sox2Ysb/-
serial sections
1
2
3
4
5
6
N
Ki67
DAPI
apical
basal
cell cycle exit

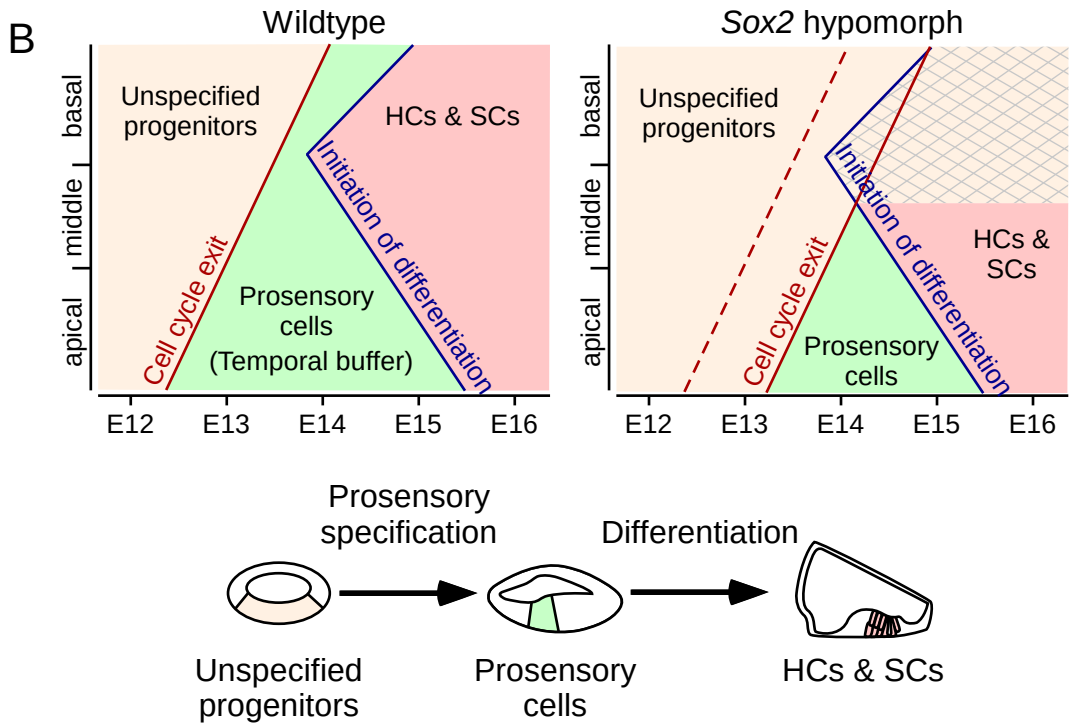
B
Wildtype
Sox2 hypomorph
basal
middle
apical
Unspecified progenitors
HCs & SCs
Cell cycle exit
Initiation of differentiation
Prosensory cells (Temporal buffer)
Prosensory cells
E12
E13
E14
E15
E16
Prosensory specification
Differentiation
Unspecified progenitors
Prosensory cells
HCs & SCs

Fig 6

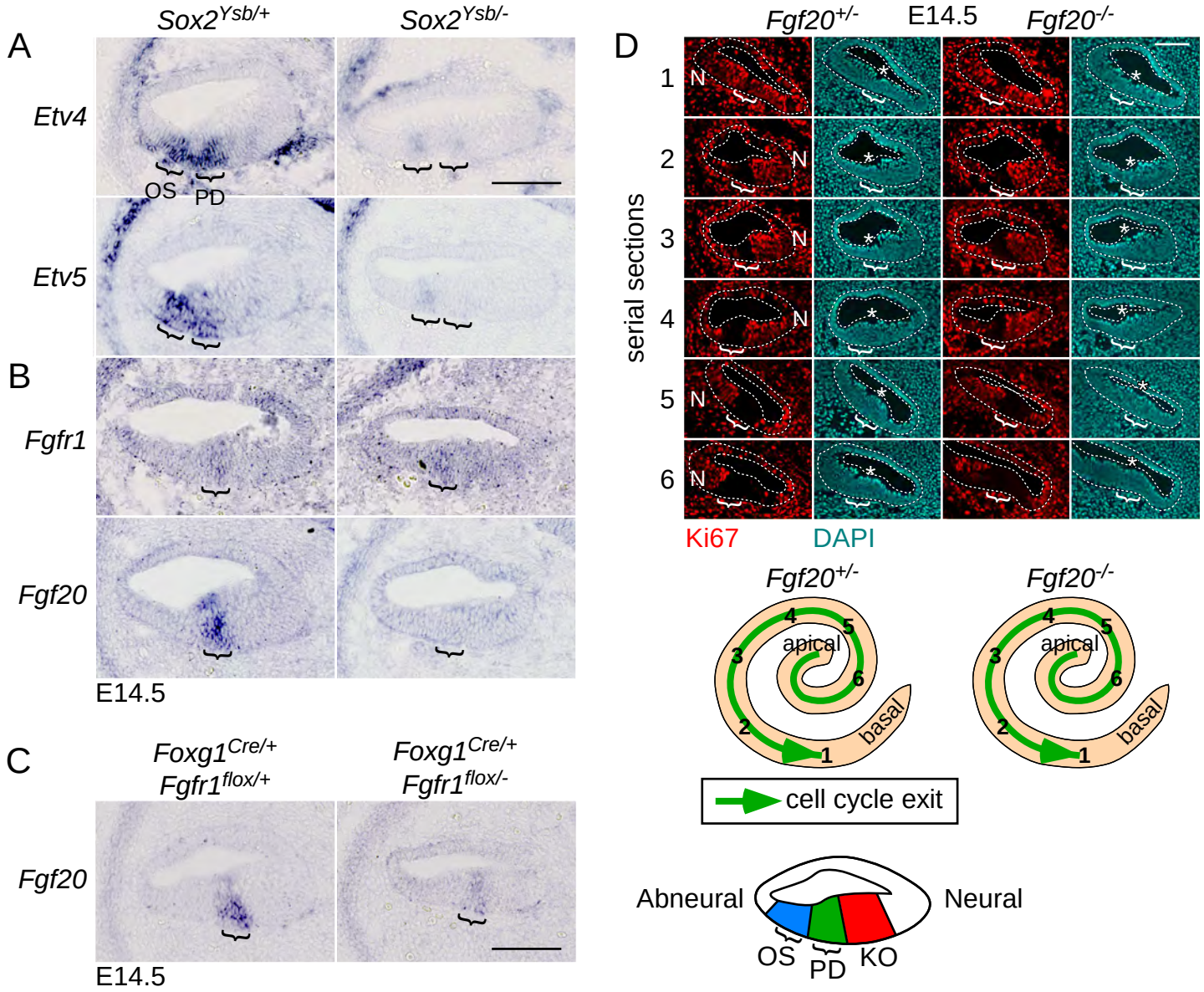
A
Sox2Ysb/+
Sox2Ysb/-
Etv4
Etv5
OS
PD
B
Fgfr1
Fgf20
E14.5
C
Foxg1Cre/+ Fgfr1flox/+
Foxg1Cre/+ Fgfr1flox/-
Fgf20
E14.5
D
Fgf20+/-
E14.5
Fgf20-/-
serial sections
1
2
3
4
5
6
N
Ki67
DAPI
Fgf20+/-
Fgf20-/-
apical
basal
cell cycle exit
Abneural
Neural
OS
PD
KO

Fig 7

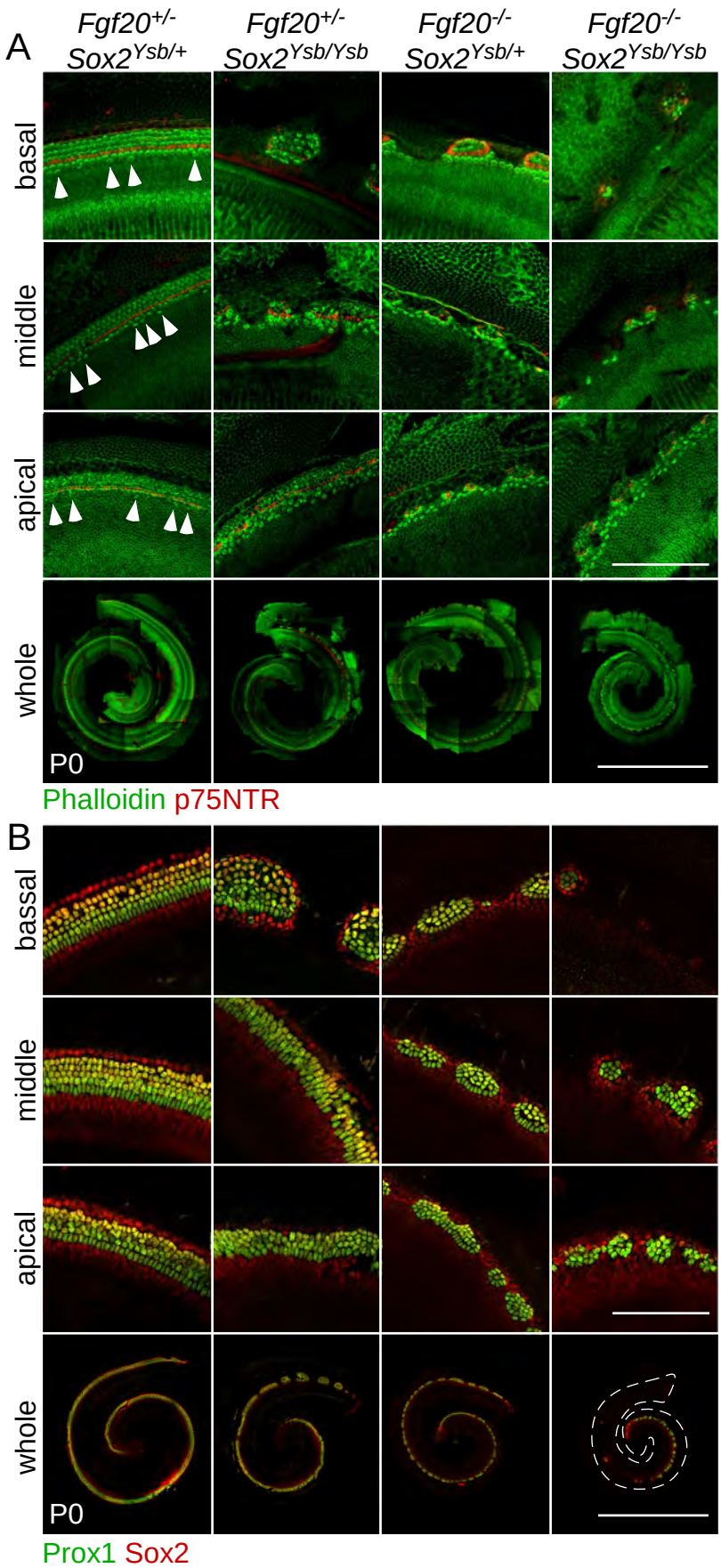
A
Fgf20+/- Sox2Ysb/+
Fgf20+/- Sox2Ysb/Ysb
Fgf20-/- Sox2Ysb/+
Fgf20-/- Sox2Ysb/Ysb
basal
middle
apical
whole
P0
Phalloidin p75NTR
B
bassal
middle
apical
whole
P0
Prox1 Sox2

Fig 8

A

2-way ANOVA	*Fgf20*	*Sox2*	Interaction
Length	p < 0.001	p < 0.001	p = 0.03
Total IHC	p < 0.001	p < 0.001	p < 0.001
IHC/100µm	p = 0.002	p = 0.2	p < 0.001
Total OHC	p < 0.001	p < 0.001	p < 0.001
OHC/100µm	p < 0.001	p < 0.001	p < 0.001
Total SC	p < 0.001	p < 0.001	p < 0.001
SC/100µm	p < 0.001	p < 0.001	p = 0.3

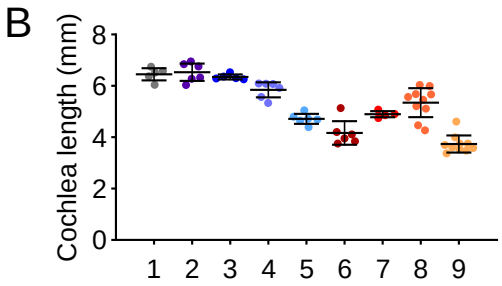

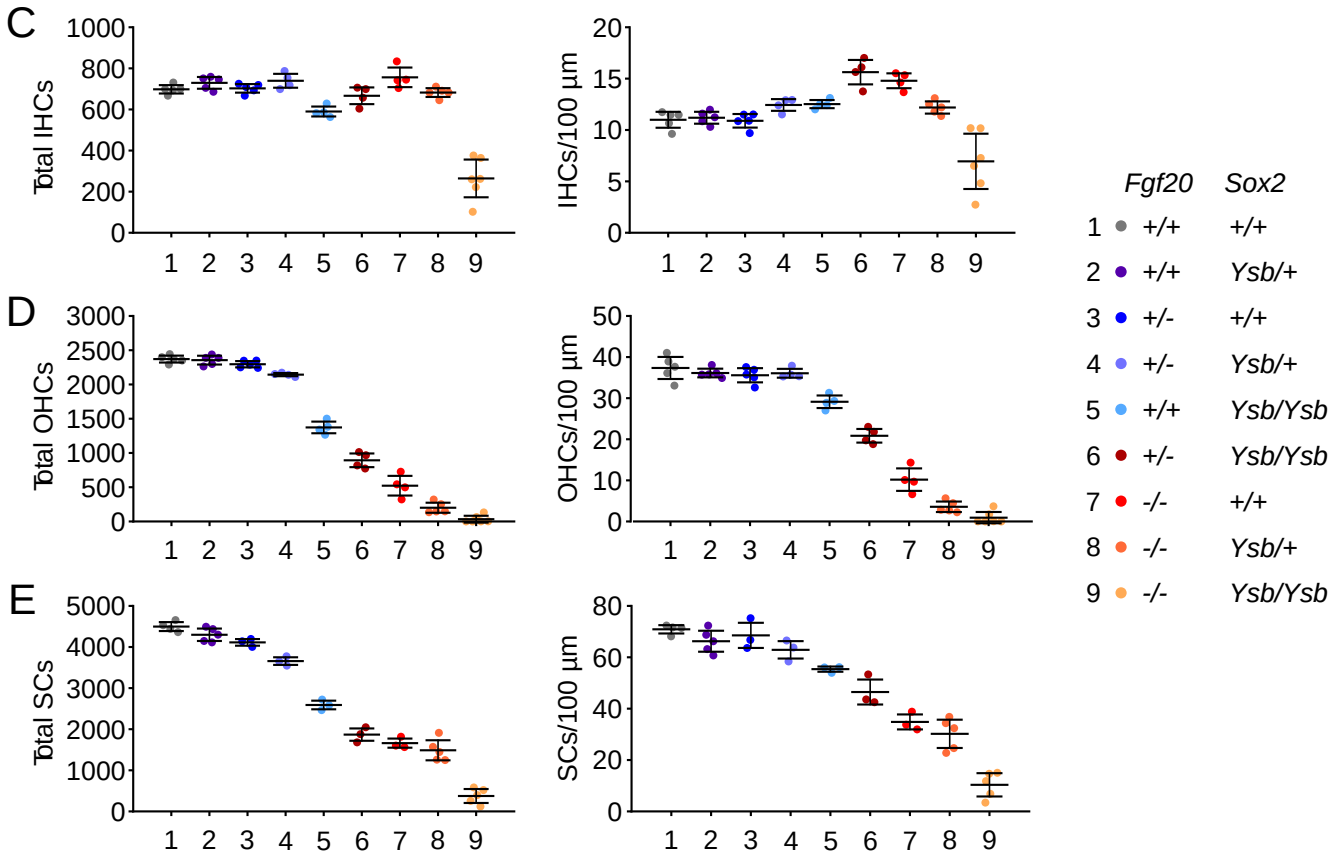

F

	1	2	3	4	5	6	7	8	9
Fgf20 / *Sox2*	+/+ +/+	+/+ Ysb/+	+/- +/+	+/- Ysb/+	+/+ Ysb/Ysb	+/- Ysb/Ysb	-/- +/+	-/- Ysb/+	-/- Ysb/Ysb
1 +/+ +/+						J	J		
2 +/+ Ysb/+						J	J		
3 +/- +/+						J	J		
4 +/- Ysb/+	O S	O S							
5 +/+ Ysb/Ysb	L OPST	L I OPS	L I OPST	L I OPS			I		
6 +/- Ysb/Ysb	L OPST	L OPST	L OPST	L OPST	OPS			L	
7 -/- +/+	L OPST	L OPST	L OPST	L OPST	OPST	OP			
8 -/- Ysb/+	L OPST	L OPST	L OPST	L OPST	OPST	JOP T	OP		
9 -/- Ysb/Ysb	L I JOPST	L I JOPST	L I JOPST	L I JOPST	L I JOPST	I JOPST	L I JOPST	L I J ST	

L cochlear length
I total IHCs
J IHCs/100 µm
O total OHCs
P OHCs/100 µm
S total SCs
T SCs/100 µm

Fig 9

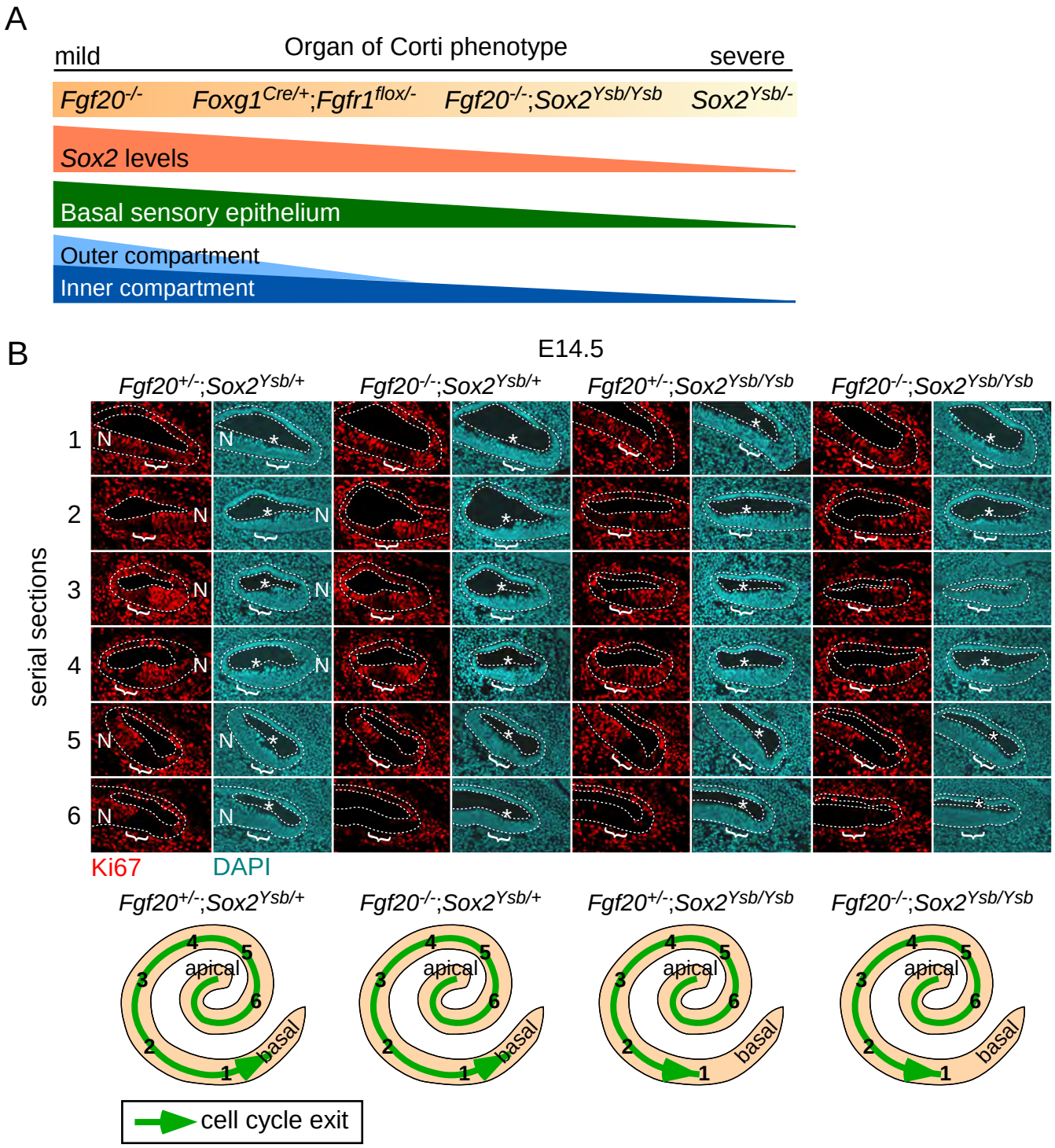
A
mild
Organ of Corti phenotype
severe
Fgf20-/-
Foxg1Cre/+;Fgfr1flox/-
Fgf20-/-;Sox2Ysb/Ysb
Sox2Ysb/-
Sox2 levels
Basal sensory epithelium
Outer compartment
Inner compartment
B
E14.5
Fgf20+/-;Sox2Ysb/+
Fgf20-/-;Sox2Ysb/+
Fgf20+/-;Sox2Ysb/Ysb
Fgf20-/-;Sox2Ysb/Ysb
serial sections
1
2
3
4
5
6
N
Ki67
DAPI
apical
basal
cell cycle exit

Fig 10

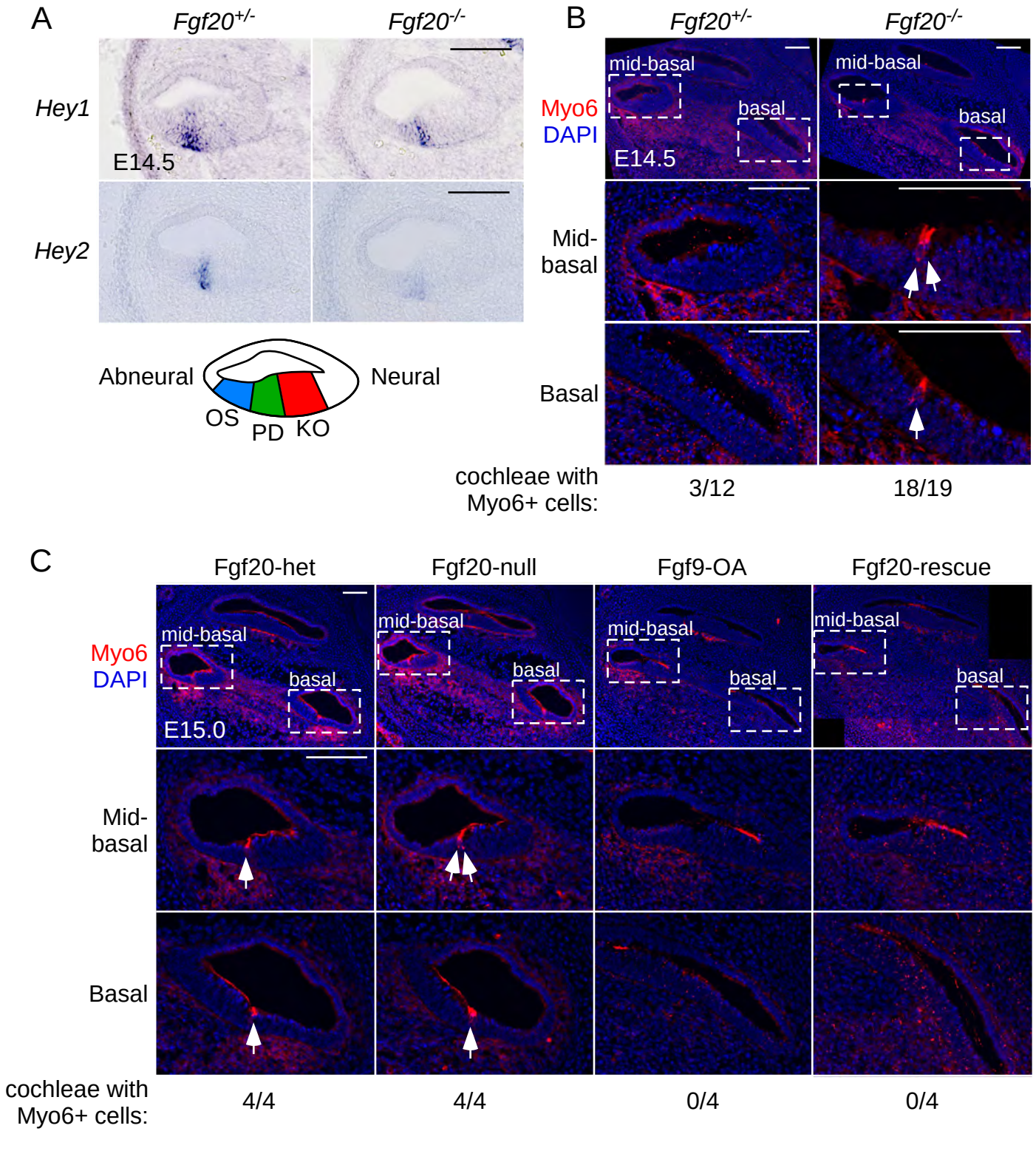
A
Fgf20+/-
Fgf20-/-
Hey1
E14.5
Hey2
Abneural
Neural
OS
PD
KO
B
Fgf20+/-
Fgf20-/-
Myo6
DAPI
mid-basal
basal
E14.5
Mid-basal
Basal
cochleae with Myo6+ cells:
3/12
18/19
C
Fgf20-het
Fgf20-null
Fgf9-OA
Fgf20-rescue
Myo6
DAPI
mid-basal
basal
E15.0
Mid-basal
Basal
cochleae with Myo6+ cells:
4/4
4/4
0/4
0/4

Fig 11

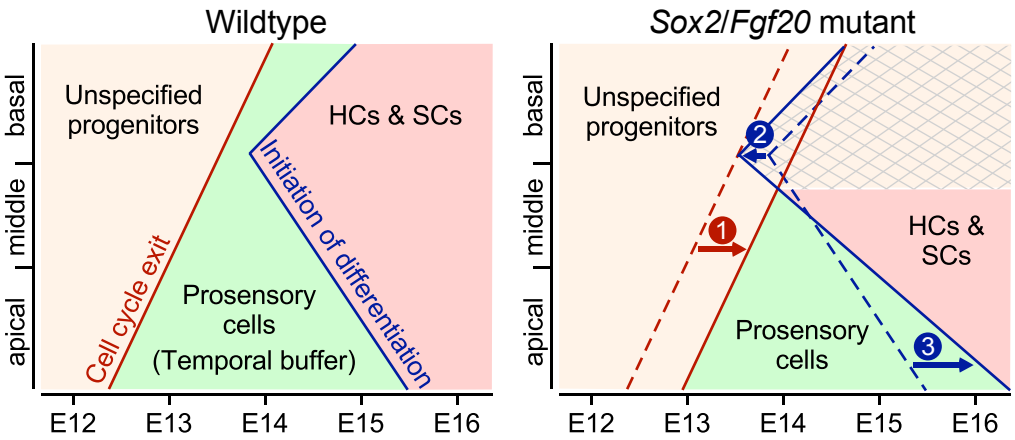
Wildtype
Sox2/Fgf20 mutant
basal
middle
apical
Unspecified progenitors
HCs & SCs
Initiation of differentiation
Cell cycle exit
Prosensory cells
(Temporal buffer)
HCs & SCs
Prosensory cells
1
2
3
E12
E13
E14
E15
E16

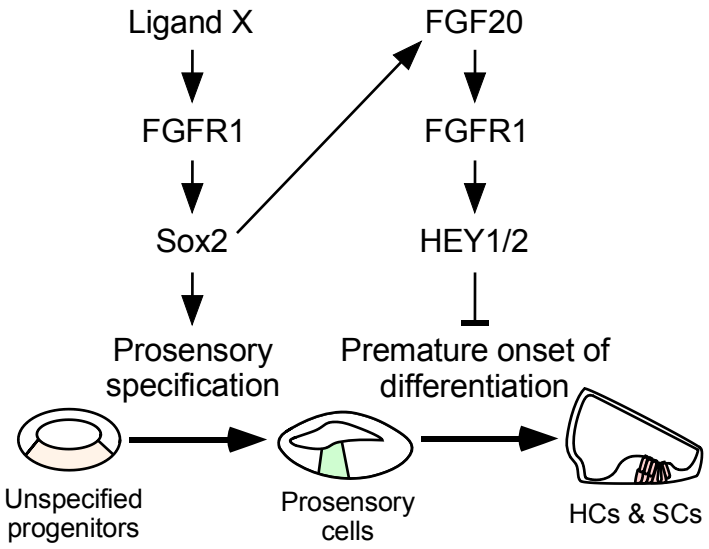
Ligand X
FGFR1
Sox2
Prosensory specification
FGF20
FGFR1
HEY1/2
Premature onset of differentiation
Unspecified progenitors
Prosensory cells
HCs & SCs